Vortex-induced vibration of floating circular cylinders with very low aspect ratio

Article *in* Ocean Engineering · April 2018
DOI: 10.1016/j.oceaneng.2018.02.019

3 authors:

Rodolfo Trentin Gonçalves
The University of Tokyo
93 PUBLICATIONS **453** CITATIONS

SEE PROFILE

Julio R Meneghini
University of São Paulo
123 PUBLICATIONS **1,490** CITATIONS

SEE PROFILE

André L. C. Fujarra
Federal University of Santa Catarina, Joinville, Brazil
119 PUBLICATIONS **758** CITATIONS

SEE PROFILE

Ocean Engineering 154 (2018) 234–251

Contents lists available at ScienceDirect

Ocean Engineering

journal homepage: www.elsevier.com/locate/oceaneng

Vortex-induced vibration of floating circular cylinders with very low aspect ratio

Rodolfo T. Gonçalves [a,*,1], Júlio R. Meneghini [b], André L.C. Fujarra [c,1]

[a] Department of Ocean Technology, Policy, and Environment, School of Frontier Sciences, The University of Tokyo, 5-1-5 Kashiwa-no-ha, Kashiwa-shi, Chiba, 277-8561, Japan

[b] Department of Mechanical Engineering, Escola Politécnica, University of São Paulo, São Paulo, SP, Brazil

[c] Department of Mobility Engineering, Joinville Campus, Federal University of Santa Catarina, Joinville, SC, Brazil

A B S T R A C T

Experiments regarding vortex-induced vibration (VIV) on floating circular cylinders with low aspect ratio were carried out in a recirculation water channel. The floating circular cylinders were elastically supported by a set of linear springs. Eight different aspect ratios were tested, namely $L/D =$ 0.2, 0.3, 0.4, 0.5, 0.75, 1.0, 1.5 and 2.0. These aspect ratios were selected to cover the aspect ratio range of the main offshore circular platforms, such as spar and monocolumn. The aim was to understand the vortex-induced motions (VIM) of such platforms; due to this, the cylinders were floating, or $m^* = 1$. The range of Reynolds number covered $2800 < \mathrm{Re} < 55{,}400$. The amplitude results showed a decrease in amplitude with decreasing aspect ratio in the in-line and in the transverse directions. The frequency results confirm a different behavior for cylinders with $L/D \leq 0.5$; in these cases, the cylinder free-end effects were predominant. The resonant behavior was no longer observed for $L/D \leq 0.2$. The decrease in Strouhal number with decreasing aspect ratio is also verified, as well as for drag and lift forces. The added mass results help to identify the end of resonance for both directions, in-line and transverse. The amplitude results for the vertical direction, roll, pitch and yaw did not affect the VIV behavior.

1. Introduction

The vortex-induced vibration (VIV) phenomenon has long been studied, and many works can be found in the literature, among which, Bearman (1984), Sarpkaya (2004) and Williamson and Govardhan (2004, 2008). The majority of these studies focused on cylinders with one degree of freedom (dof), i.e. the cylinders vibrate only in the transverse direction of the incident flow. Recently, the cylinders with 2dof have become an object of studies due to the offshore demand; for example, the riser systems connected to the offshore platforms. These works regarded the high aspect ratio cylinders. The high aspect ratio cylinders characteristic is that the submerged length is much longer than the characteristic diameter of the cylinder, $L/D > 13$ (where L/D represents the aspect ratio value, L is the immersed length of the cylinder and D is the respective characteristic diameter); see for example Jauvtis and Williamson (2004).

Another demand of the offshore industry also raised the interest in the VIV around floating cylinders with low aspect ratio, $0.3 < L/D < 6.0$, and small mass ratio, $m^* < 6.0$. This specific subject was called vortex-induced motions (VIM), whose motivation has been the high velocity of the incident current on circular offshore platforms, particularly cases of a spar, $1.5 < L/D < 6.0$, see works by Dijk et al. (2003) and Finn et al. (2013); and monocolumn, $0.2 < L/D < 0.5$, see work by Gonçalves et al. (2010). VIM has also been studied on multi-column platforms, such as semi-submersible and tension leg platforms (TLP), see works by Gonçalves et al. (2012c, 2013b, 2018) and Liu et al. (2016, 2017); in these cases of platforms, the columns can also be considered cylinders with low aspect ratio, $1.0 < L/D < 2.2$.

Floating circular platforms present a large characteristic diameter associated with a large natural period of motions in the horizontal plane; therefore, these systems are subjected to VIM that can directly affect the fatigue life of riser and mooring systems. In this context, our aim here is to understand, with experiments in a circulating water channel, the VIV around floating circular cylinders, $m^* = 1.0$, with very low aspect ratio, $0.2 \leq L/D \leq 2.0$, as a motivation for better understanding the VIM of platforms.

The work tries to complete the studies previously conducted for the flow around a stationary cylinder with very low aspect ratio presented by Gonçalves et al. (2015). In the latter, the particle image velocimetry (PIV) measurements and the power spectrum density (PSD) of forces showed

* Corresponding author.
E-mail addresses: goncalves@edu.k.u-tokyo.ac.jp (R.T. Gonçalves), jmeneg@usp.br (J.R. Meneghini), andre.fujarra@ufsc.br (A.L.C. Fujarra).

[1] formerly at the TPN – Numerical Offshore Tank laboratory, Department of Naval Architecture and Ocean Engineering, Escola Politécnica, University of São Paulo, São Paulo, SP, Brazil.

https://doi.org/10.1016/j.oceaneng.2018.02.019
Received 5 July 2017; Received in revised form 9 January 2018; Accepted 5 February 2018

Nomenclature

β	Blockage coefficient
γ	Modal form factor
ρ	Fluid density
ζ_s	Structural damping
ζ_w	Damping coefficient in still water
$A_x/(\gamma D)$	Characteristic nondimensional motion amplitude in the in-line direction
$A_y/(\gamma D)$	Characteristic nondimensional motion amplitude in the transverse direction
C_x	Nondimensional drag coefficient
C_{x-rms}	Non-time dependent oscillatory drag coefficient
C_y	Nondimensional lift coefficient
C_{y-rms}	Non-time dependent lift coefficient
D	Characteristic diameter
$\mathscr{F}[]$	Fast Fourier transform operator
F_{Hx}	Total hydrodynamic force in the in-line direction
F_{Hy}	Total hydrodynamic force in the transverse direction
f_0	Natural frequency in still water, both in in-line and transverse directions
f_{0x}	Natural frequency of the system in still water in the in-line direction
f_{0y}	Natural frequency of the system in still water in the transverse direction
f_s	Vortex-shedding frequency
f_x	Oscillation frequency in the in-line direction
f_y	Oscillation frequency in the transverse direction
GM	Metacentric height
H	Water level of the water channel
h	Distance between the cylinder free end and the bottom of the water channel
KG	Vertical center of gravity position
k_x	Stiffness in the in-line direction
k_y	Stiffness in the transverse direction
L	Immersed length
L_q	Length of the stiffness support
m^*	Mass ratio
m_{ax}	Added mass in the in-line direction
m^*_{ax}	Added mass coefficient in the in-line direction
m_{ay}	Added mass in the transverse direction
m^*_{ay}	Added mass coefficient in the transverse direction
m_d	Displaced mass
m_s	Structural mass
L/D	Aspect ratio
$\mathscr{R}[]$	Real part of the complex number
Re	Reynolds number
St	Strouhal number
t	Time
U	Flow velocity
V_r	Reduced velocity
W	Width of the water channel
W_q	Width of the stiffness support
x	In-line direction axis or displacement in the in-line direction
y	Transverse direction axis or displacement in the transverse direction

different behavior for cylinders with $L/D \leq 0.5$, in which cases the free-end effects were predominant. Even without von Kármán street main characteristics around most of the span length of the cylinder, in the range of $0.2 < L/D \leq 0.5$, the vortex shedding around it was capable of producing alternating forces in the transverse direction. Therefore, alternating forces were not observed in the transverse direction for cylinders with $L/D \leq 0.2$.

Section 2 presents a background of VIM phenomenon of offshore platforms as well as a background of VIV of cylinders with low aspect ratio. Section 3 shows the experimental setup of the tests performed. The analysis methodology of the tests is presented in Section 4. Section 5 presents the experimental results comprising nondimensional amplitudes for the 6dof and the frequencies in both transverse and in-line direction. Additionally, the PSD of the motions is given for supporting the discussions and conclusions. In the same chapter, drag and lift forces and added mass coefficient are also discussed. All the results are shown as a function of the reduced velocity, $V_r = U/f_0D$ (where U represents the flow velocity, and f_0 is the natural frequency in still water in the transverse direction). Finally, Section 6 presents the general conclusions and perspectives of the current work.

2. Background

2.1. Vortex-induced motion of offshore platforms

The study of VIM has become of utmost importance since offshore platforms were placed in the Gulf of Mexico, USA, where the strong loop currents triggered vigorous motions due to vortex shedding. In this region, spar platforms were a good solution to explore and to produce hydrocarbons at deep water levels. However, the cylindrical shape of this type of platform with a high level of current speeds is susceptible to synchronized vortex shedding that induces large motion of the order of its diameter dimension.

Among the first experimental VIM studies of spar platforms, works by Dijk et al. (2003) and Finn et al. (2013), for example, can be highlighted. Their purpose was to verify the influence of the hull geometry and appendages. The maximum amplitudes in the transverse direction observed were around 70% of the characteristic diameter. The typical aspect ratio of the spar platforms is around the range of $1.5 < L/D < 6.0$.

The VIM of monocolumn platforms showed to be important even considering their lower aspect ratio. The typical aspect ratio of a monocolumn platform is around the range of $0.2 < L/D < 0.5$. The work by Gonçalves et al. (2010) observed transverse motion amplitudes around 100% of the characteristic diameter and significant coupled motion between in-line and transverse motions, characterized by eight-shape trajectories.

Recently, the increase in the demand for the multi-column platforms as a solution for exploring ultra-deep-water level oil fields demands a better understanding of the VIM phenomenon in this kind of platforms. The interaction of the vortex shedding surrounding each column promotes large amplitudes of VIM, around 40% of the characteristic diameter of the columns as shown, among others, by Gonçalves et al. (2012c, 2013b, 2018) and Liu et al. (2016, 2017).

The large amplitudes caused by VIM combined with the periodic motion characteristics decrease the fatigue life of risers and mooring lines implying high costs for the platform project. Antony et al. (2017) presented costs saving associated with improving VIM prediction accuracy, and highlighted the importance of quantifying the VIM of floating offshore platforms. This paper thus tries to help designers to understand the VIM phenomenon fundamentally, i.e. from basic VIV tests of very low aspect ratio cylinders, since VIM is most studied for a particular platform hull, which makes it difficult to extrapolate the results in a general way.

2.2. Vortex-induced vibration of cylinders with low aspect ratio cylinders

As commented before, the VIV studies of a cylinder with 2dof are

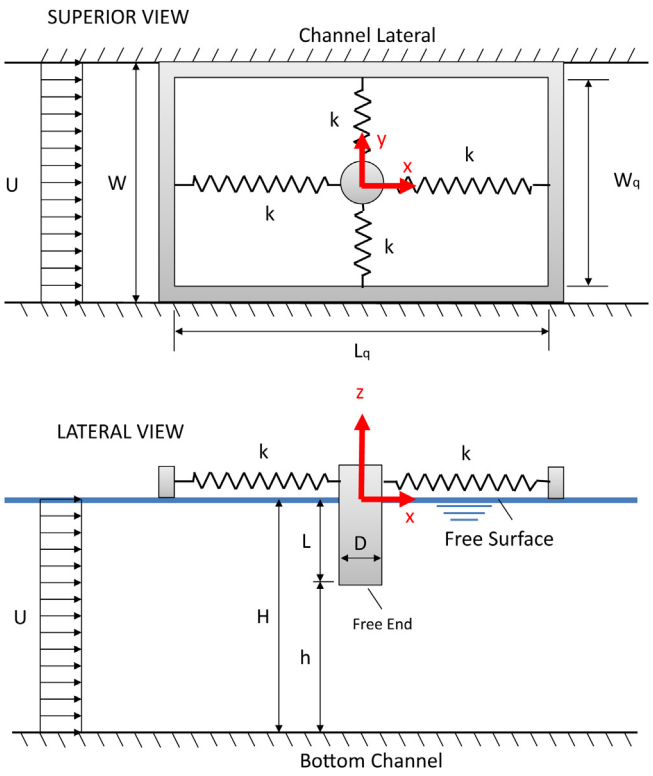

Fig. 1. Experimental setup and dimensional parameters.

Table 1
Dimensional parameters of the tests with different aspect ratios.

L/D	H [mm]	h [mm]	β
2.0	536	286	0.08
1.5	536	349	0.06
1.0	536	411	0.04
0.75	536	442	0.03
0.5	536	474	0.02
0.4	536	486	0.02
0.3	536	499	0.01
0.2	536	511	0.01

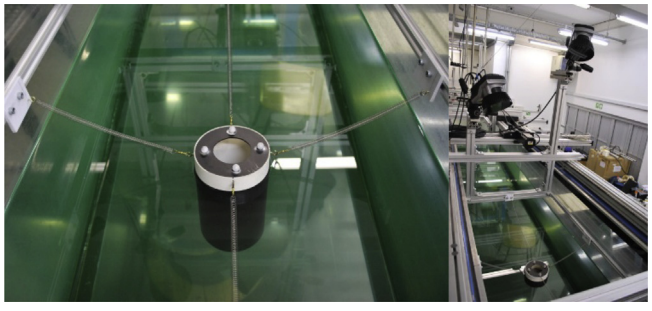

Fig. 2. Illustration of the floating cylinder elastically supported by a set of four springs and experimental arrangement of optical motion capture system.

more recent than 1dof ones. In the offshore scenario, cylinders with 2dof and small mass ratio, $m^* < 6$, are necessary since the largest number of cases is cylinder immersed in water.

Particular attention has been given to long cylinders with $m^* \approx 2.5$. This value is a typical value for risers. Pesce and Fujarra (2000) presented 2dof VIV results for long flexible cantilever bar with $m^* = 2.4$ and $L/D = 94.5$; the results showed significant amplitudes in the transverse

Fig. 3. Illustration of PVC models of the cylinders with low aspect ratio.

Table 2
Inertia properties of the cylinders with different aspect ratios.

L/D	m [g]	KG [mm]	GM [mm]
2.0	3068	57.7	71.2
1.5	2300	42.2	56.7
1.0	1534	27.0	43.3
0.75	1150	19.6	37.7
0.5	767	12.5	34.3
0.4	614	10.0	34.5
0.3	460	7.9	36.9
0.2	307	6.8	44.8

Table 3
Natural frequencies in the still water of the tests with different aspect ratios obtained from decay tests.

L/D	f_{0x} [Hz]	f_{0y} [Hz]	f_{0z} [Hz]	f_{0roll} [Hz]	f_{0pitch} [Hz]	f_{0yaw} [Hz]	ζ_w [%]
2.0	0.10	0.10	0.94	0.98	1.01	0.50	4.64
1.5	0.12	0.12	1.08	1.41	1.41	0.57	3.97
1.0	0.14	0.15	1.28	1.56	1.59	0.70	3.31
0.75	0.17	0.17	1.41	1.64	1.69	0.81	3.74
0.5	0.22	0.23	1.61	1.89	2.00	1.04	4.23
0.4	0.25	0.26	1.72	2.04	2.17	1.12	3.97
0.3	0.28	0.30	1.92	2.13	2.27	1.22	4.22
0.2	0.34	0.35	2.08	2.08	2.27	1.30	4.39

Table 4
Parameters of the tests for each aspect ratio condition.

L/D	U [m/s]	V_r	$Re \times 10^{-4}$	Fr_L
2.0	0.02 → 0.13	1.82 → 9.91	0.28 → 1.57	0.01 → 0.08
1.5	0.03 → 0.14	2.23 → 9.45	0.41 → 1.75	0.02 → 0.10
1.0	0.04 → 0.22	2.39 → 11.73	0.55 → 2.70	0.04 → 0.20
0.75	0.02 → 0.30	1.11 → 13.69	0.30 → 3.72	0.03 → 0.31
0.5	0.06 → 0.39	1.97 → 13.34	0.71 → 4.83	0.07 → 0.49
0.4	0.06 → 0.40	1.86 → 12.83	0.72 → 5.02	0.08 → 0.57
0.3	0.07 → 0.43	2.10 → 12.29	0.91 → 5.35	0.12 → 0.71
0.2	0.09 → 0.44	2.03 → 10.21	1.10 → 5.54	0.18 → 0.89

direction due to the presence of a 2T – triple vortices formation around the cylinder. Later, Jauvtis and Williamson (2004) proved the existence of the 2T structure due to the existence of 2dof and small mass ratio values; in this work, a rigid vertical cylinder supported by an elastic base with $m^* = 2.6$ and $L/D = 10$ was studied. The presence of an initial, super-upper and the lower branch were observed to be different as compared with $m^* > 6$. Later, Stappenbelt and Lalji (2008) confirmed this behavior for a rigid vertical cylinder supported by an elastic base with $m^* = 2.4$ and $L/D = 8$. Other important studies for 2dof and small mass ratio can be cited, such as Blevins and Coughran (2009), for a vertical rigid cylinder supported by an elastic base with $m^* = 2.6$ and $L/D = 17.8$; Freire and Meneghini (2010), for a vertical rigid pivoted

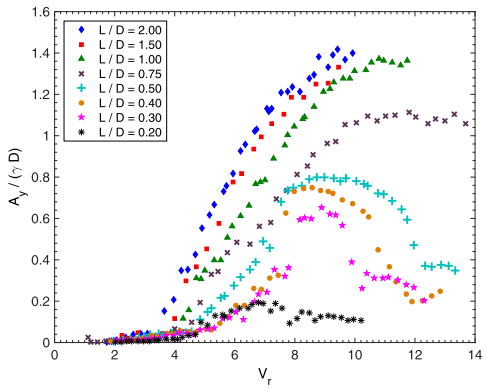

Fig. 4. Characteristic motion amplitude in the transverse direction ($A_y/(\gamma D)$) as a function of reduced velocity (V_r) for cylinders with mass ratio of $m^* = 1.00$ and eight different aspect ratios ($L/D \leq 2.00$).

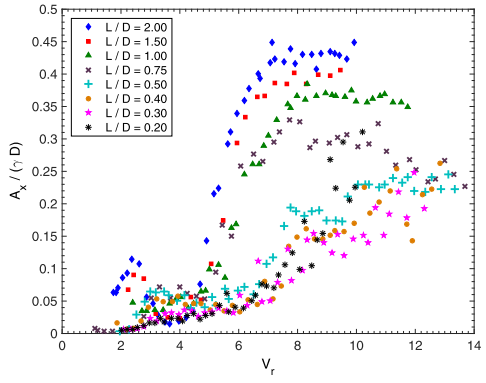

Fig. 5. Characteristic motion amplitude in the in-lie direction ($A_x/(\gamma D)$) as a function of reduced velocity (V_r) for cylinders with mass ratio of $m^* = 1.00$ and eight different aspect ratios ($L/D \leq 2.00$).

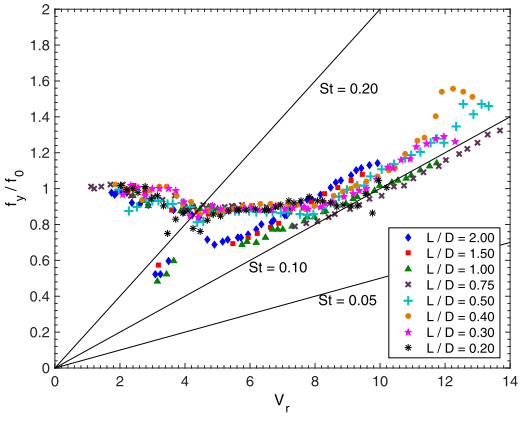

Fig. 6. Ratio between the transverse motion frequency and the natural transverse frequency in still water (f_y/f_0) as a function of reduced velocity (V_r) for cylinders with mass ratio of $m^* = 1.00$ and eight different aspect ratios ($L/D \leq 2.00$).

cylinder with $m^* = 2.8$ and $L/D = 21.9$; and Franzini et al. (2013), for a vertical rigid cylinder supported by elastic base with $m^* = 2.6$ and $L/D = 13.0$. In all the works cited about the VIV on 2dof cylinders with small mass ratio, transverse amplitudes were almost the same, independently of the aspect ratio, $L/D > 8$, and no free end effects were taken into account then.

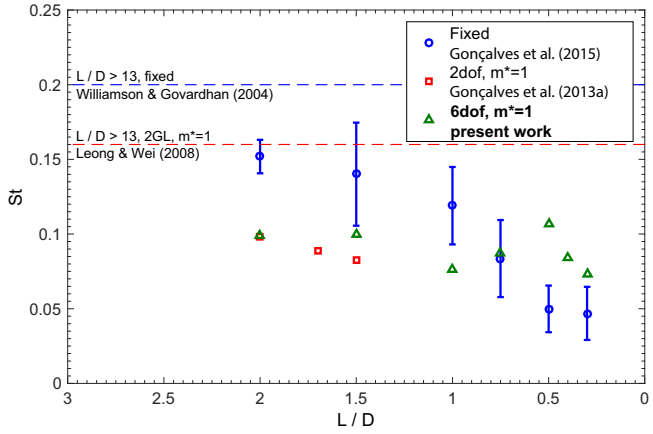

Fig. 7. Strouhal "like" number (St) as a function of aspect ratio (L/D) for cylinders with low aspect ratio for fixed and VIV cases.

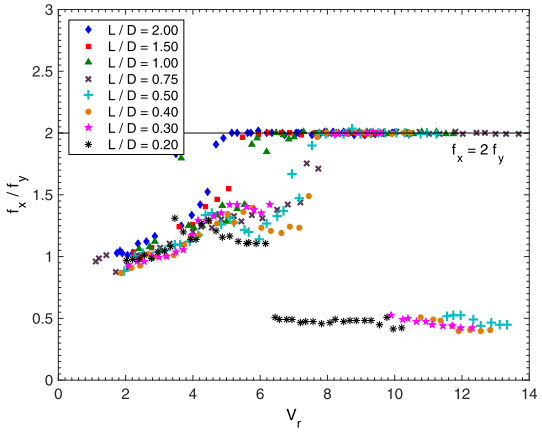

Fig. 8. Ratio between in-line and transverse motion frequencies (f_x/f_y) as a function of reduced velocity (V_r) for cylinders with mass ratio of $m^* = 1.00$ and eight different aspect ratios ($L/D \leq 2.00$).

In Morse et al. (2008), the free-end effect was investigated by considering a rigid cylinder supported elastically with $L/D < 8$ and free to oscillate only in the transverse direction of the flow. Against expectation, the transverse amplitudes of oscillation for the cylinder equipped with an endplate were no higher than those presented by the same cylinder without it. The conclusion is that the free end effects are important in the VIV of cylinders with $L/D < 8$. The presence of free end affected the lower branch behavior and kept the transverse amplitudes still significant for high reduced velocities, and it is not possible to observe a sudden drop in the amplitudes.

Studies on VIV of low aspect ratio cylinders started due to the demand for floating offshore platforms, characterized by low aspect ratio structures $L/D < 6$. Another important characteristic of these units is the very small mass ratio, typical floaters, such as a spar, monocolumn, and the semisubmersible platforms have $m^* \approx 1$; and TLP platforms have $m^* < 1$ due to the presence of the tensioned tendons. Blevins and Coughran (2009) also presented results for a cylinder with mass ratio value around one, $m^* \approx 1$, and $L/D = 17.8$. This result is crucial to compare the results from floating cylinders. The results by Blevins and Coughran (2009) showed that the lower branch is not present for this mass ratio, a behavior distinct of that presented in the cylinders with $m^* \approx 2.5$. These previous works show the importance of understanding both effects: the very low aspect ratio and floating cylinder mass ratio characteristic, $m^* \approx 1$.

Few studies are found in the literature studying the VIV on cylinders

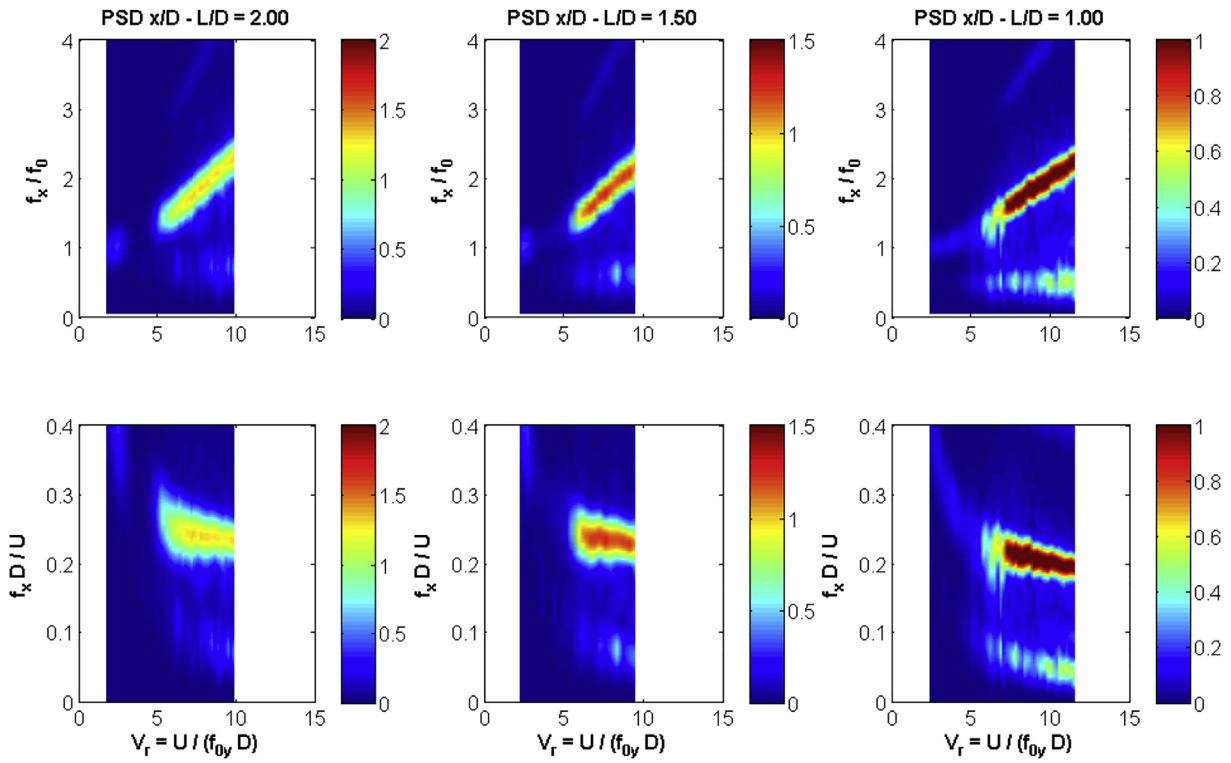

Fig. 9. PSD of the motion in the in-line direction as a function of V_r for cylinders with mass ratio of $m^* = 1.00$ and different aspect ratios ($1.00 \leq L/D \leq 2.00$).

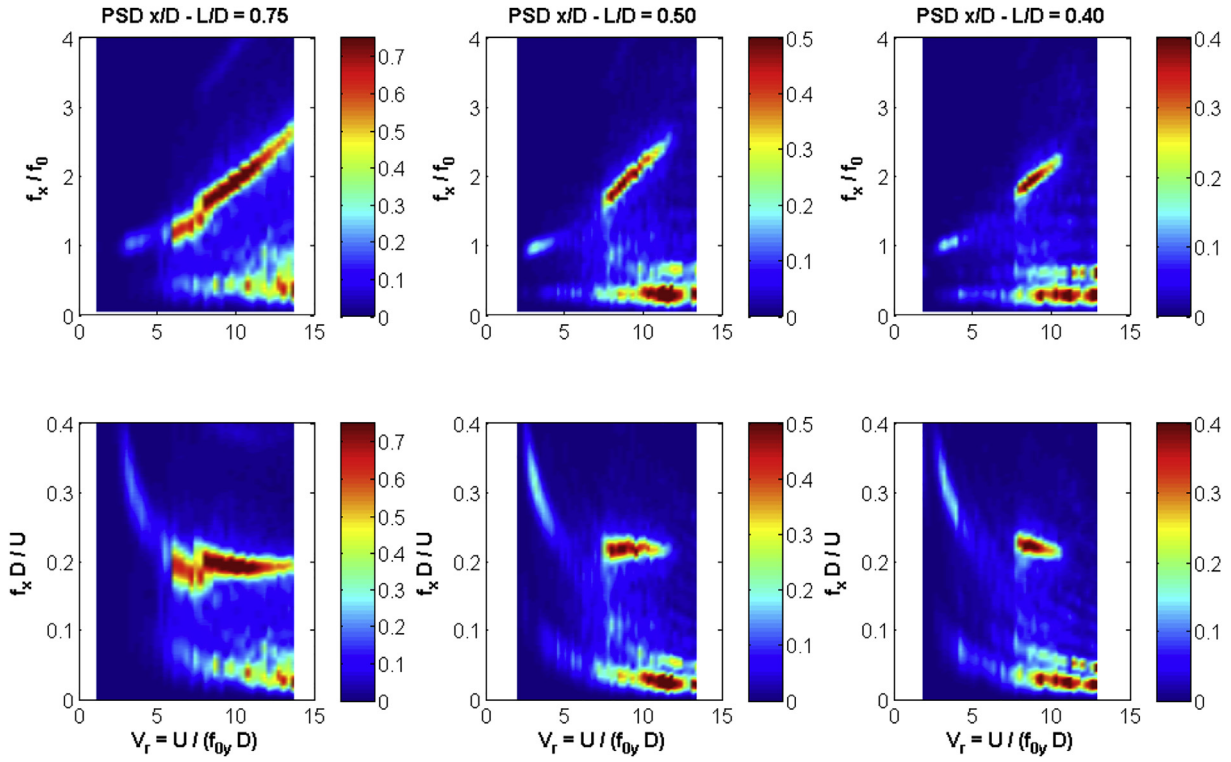

Fig. 10. PSD of the motion in the in-line direction as a function of V_r for cylinders with mass ratio of $m^* = 1.00$ and different aspect ratios ($0.40 \leq L/D \leq 0.75$).

with very low aspect ratio and small mass ratio. The studies about 2dof VIV of small mass ratio cylinders with high aspect ratio were cited in the previous paragraph. The behavior of very low aspect ratio cylinders was further studied only for the flow around fixed cylinder cases mounted on a surface; in these cases, the cylinders do not pierce the free surface. A review of the flow above the free end of a surface-mounted finite-height circular cylinder can be found in Sumer (2013). The aspect ratio $L/D = 2$ was defined as the threshold value in which the three-dimensional (3D) structures around the cylinder free end become more important than the typical two-dimensional (2D) vortex structures along the vertical span of

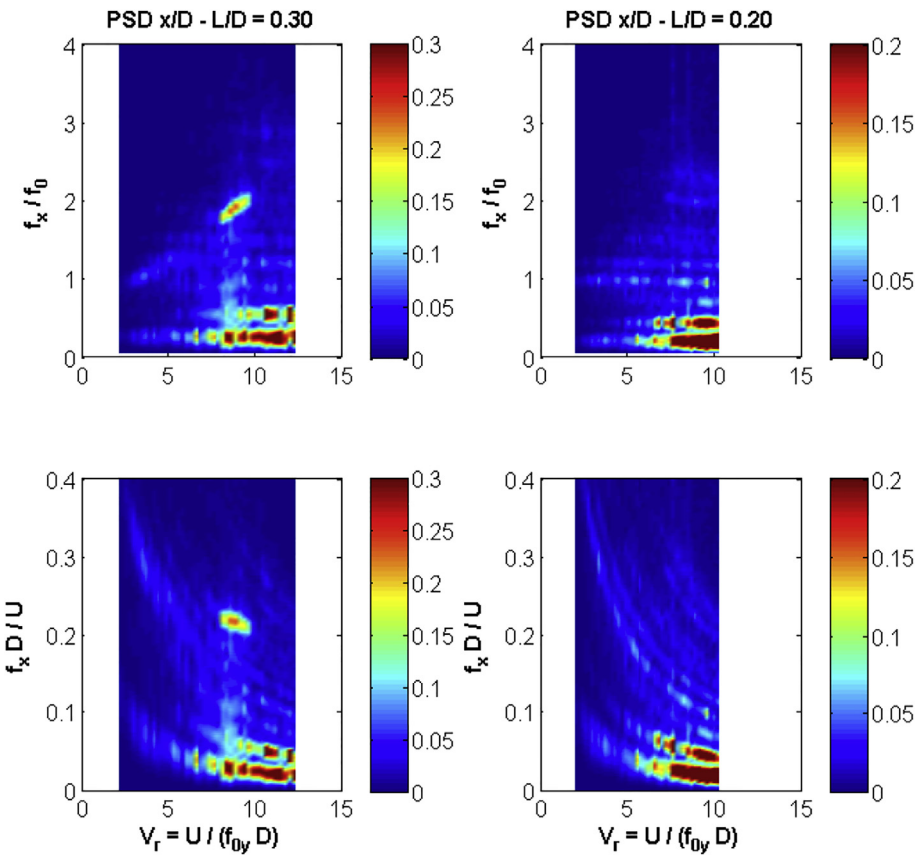

Fig. 11. PSD of the motion in the in-line direction as a function of V_r for cylinders with mass ratio of $m^* = 1.00$ and different aspect ratios ($0.20 \leq L/D \leq 0.30$).

the cylinder, as commented by some authors in the review. The typical von Kármán street cannot be determined, and symmetric structures can be observed for $L/D < 2$.

One of the goals here is to complement the results submitted by Gonçalves et al. (2015). Hence, experiments on the flow around stationary circular cylinders with very low aspect ratio piercing the water free surface were carried out. Eight different aspect ratios were tested, $0.2 \leq L/D \leq 2.0$; no end-plates were employed. Forces were measured using a six-degree-of-freedom load cell, and the Strouhal number was inferred from the transverse force fluctuation frequency. The range of Reynolds number covered $10\,000 < \mathrm{Re} < 50\,000$. The results showed a decrease in drag force coefficients with decreasing aspect ratio, as well as a decrease in Strouhal number with decreasing aspect ratio. The PIV measurements and the PSD of forces showed different behavior for cylinders with $L/D = 0.5$, in which cases the free-end effects were predominant. Even without von Kármán street main characteristics around the length of the cylinder, in the range of $0.2 < L/D \leq 0.5$, the vortex shedding around it was capable of producing alternating forces in the transverse direction. Therefore, alternating forces were not observed in the transverse direction for cylinders with $L/D \leq 0.2$. The phenomenology around fixed cylinders can be used to better understand the behavior for 2dof. Recently, Fukuoka et al. (2016) performed similar experiments to evaluate the effects of the free surface and end cell on flow around a finite circular cylinder with low aspect ratio, and the results were similar as compared with the previous work cited for the aspect ratio teste $1 \leq L/D \leq 4$.

Fundamental VIV experiments of floating circular cylinders became necessary since the previous VIM tests of offshore platforms took into account the complex details of the hull, such as strakes, fairleads, and other hydrodynamic appendages. This modification in the cylinder geometry from a bare hull changed the vortex formation around the cylinders, and the phenomenon could not be understood as a whole, and it is specific for each particular platform. Sanchis et al. (2008) experimented a floating cylinder with $L/D = 6$ and showed, for a small range of reduced velocity tested $4 < V_r < 8$, amplitudes in the transverse direction around 100% of the characteristic diameter for the highest velocity tested. Wang et al. (2009), aiming to understand the hard tank section of a spar platform, performed VIV tests on a floating cylinder with $L/D = 2.4$ for a range of $3 < V_r < 7$; the highest transverse amplitude was around 80% of the characteristic diameter for the highest reduced velocity tested. Recently, Fujiwara et al. (2013) performed VIV tests on a floating cylinder with $L/D = 3$ for a wide range of reduced velocities $2 < V_r < 11$; in these experiments, the transverse amplitudes reached around 120% the characteristic diameter, and the absence of the lower branch was observed. In Blevins and Coughran (2009), the absence of the lower branch was also observed for a cylinder with $L/D = 17.8$ and $m^* \approx 1$. Additionally, Someya et al. (2010) was the first work to draft a schematic of the structures around the free end of a cylinder with $L/D = 5$ undergoing VIV; the authors proposed that the 3D structures around the free end were tip vortex and they were those responsible for affecting the VIV of cylinders with low aspect ratio.

The few results of VIV of floating cylinders with low aspect ratio cited ranging $2.4 \leq L/D \leq 6$ did not show a great difference in amplitudes when compared with the high aspect ratio case, for example. Our goal to fill this lack in the literature was motivated by the monocolumn platforms $L/D \approx 0.4$.

It is possible to find some works in the literature about the VIV of very low aspect ratio cylinders, $L/D \leq 2.0$. For example, Gonçalves et al. (2012b, 2013a) present a series of fundamental experiments on 2dof VIV of circular cylinders with very low aspect ratio, $0.3 \leq L/D \leq 2.0$, and small mass ratio values, namely, 1.00, 2.62, and 4.36. Conversely, to what would be expected for cylinders with very low aspect ratio, the results showed large motions in the transverse direction with maximum amplitudes around 150% of the characteristic diameter for cylinders with $L/D = 2$, despite being smaller when the aspect ratio is reduced. The response amplitudes presented high values around 40% of the

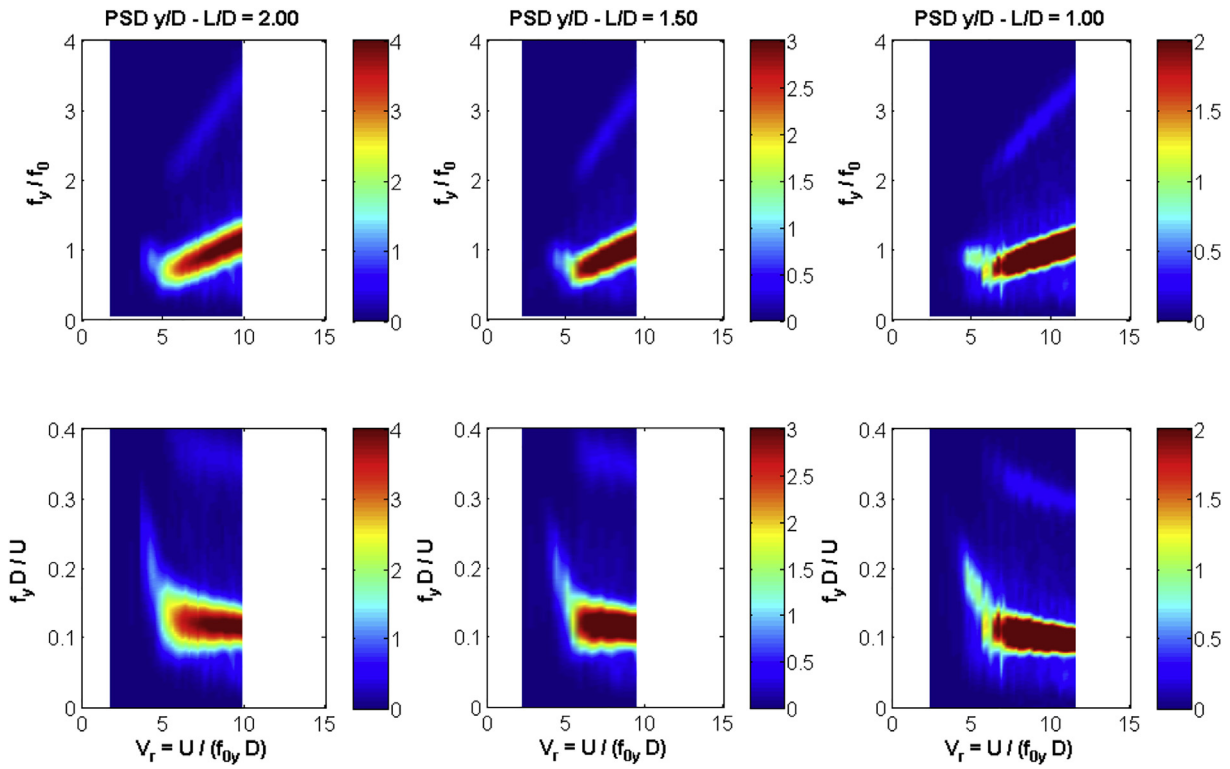

Fig. 12. PSD of the motion in the transverse direction as a function of $\mathbf{V_r}$ for cylinders with mass ratio of $\mathbf{m^* = 1.00}$ and different aspect ratios ($\mathbf{1.00 \leq L/D \leq 2.00}$).

characteristic diameter in the in-line direction. The case of $m^* \approx 1$ deserves more attention because it shows lower amplitude than the cases with the same aspect ratio and larger mass ratio. This counter-intuitive behavior seems to be related to the energy transferring process from the steady stream to the oscillatory hydro-elastic system. The case of $m^* \approx 1$ was studied only for cylinders with $L/D = 2$ and $L/D = 1.5$; tests are still necessary for lower values of aspect ratio.

Rahman & Thiagarajan (2015) and Rahman et al. (2016) performed experimental and numerical studies, respectively, on 1dof VIV of low aspect ratio cylinders in the range of $0.5 \leq L/D \leq 13$ and mass ratio value $m^* = 1.6$. The response amplitude was observed to decrease as the aspect ratio reduced. The decrease in response amplitude was found to be accompanied by a reduction in the correlation length of vortex shedding. The decreasing trend is also followed by the results measured for drag and lift force. This is the same behavior pointed out by the previous works by Gonçalves et al. (2013a) for 2dof cases. Complementing these works, Zhao and Cheng (2014) performed CFD simulations for 1dof VIV of a circular cylinder with $1 \leq L/D \leq 20$ and mass ratio $m^* = 2$ to try to understand the 3D structures around the cylinder free end. The vortices that were shed from the cylinder with low aspect ratio $L/D = 2$ and $L/D = 1$ were found to be generated from the cylinder free end and convected toward the top end of the cylinder by the up-wash velocity. The wake flow in a vibrating cylinder with $L/D \geq 5$ includes the vortex shedding flow at the top part of the cylinder and the end-induced vortex shedding near the free end of the cylinder.

After this literature review, it is possible to verify the importance of studying the VIV of floating circular cylinders with very low aspect ratio, a still little explored subject in the literature.

3. Experimental setup

All the experiments were carried out in a recirculating water channel at the Fluid & Dynamics Research Group Laboratory (NDF) facility of the University of São Paulo (USP), Brazil. The water channel has a test section 0.7 m wide, 0.9 m deep and 7.5 m long. The flow speed U is variable up to 0.4 m/s, allowing for tests with different values of Reynolds number and reduced velocity with a turbulence intensity of less than 3%, obtained from velocity and turbulence profiles measured with hot-film anemometers by Assi (2005).

The floating cylinder was elastically supported by a set of four springs with the same stiffness parameter, $k = 0.73$ N/m, in a rectangular support with dimensions $L_q = 1090$ mm and $W_q = 610$ mm, length and width respectively, as can be seen in Fig. 1 and Table 1. The springs were fixed in the model above 20 mm from the water line to prevent them from touching the water in any condition. The vertical distance between the point where the springs were attached to the rectangular support and the point where the springs were fixed on the model was 100 mm; therefore, the spring angles were smaller than 10°. Due to these small angles, the restoration of the system still can be considered linear in the range of the displacements of the tests performed.

The models were made of polyvinyl chloride (PVC) with external diameter $D = 125$ mm. The cylinder is free to move in the 6dof. The motions were measured using an optical motion capture system, Qualisys. Details of the position of the camera can be seen in Fig. 2. Due to the small volume of control measured during the tests, the standard deviation error of measurements is lower than 0.1 mm.

Eight different cylinders were built, one for each aspect ratio tested, namely: $L/D =$ 0.20; 0.30; 0.40; 0.50; 0.75; 1.00; 1.50 and 2.00; see Fig. 3. The loading condition was adjusted changing the ballast inside the models. The water height of the channel was kept constant during the tests, $H = 536$ mm; thus, the distance between the cylinder free end and the bottom of the water channel, h, depending on the aspect ratio, as can be seen in Table 1.

The blockage coefficient can be defined as $\beta = LD/HW$, where H is the water height, and W is the width of the water channel. For all the cases, the blockage coefficient was smaller than 8%, as observed in Table 1.

The mass property, vertical center of gravity position (KG) and

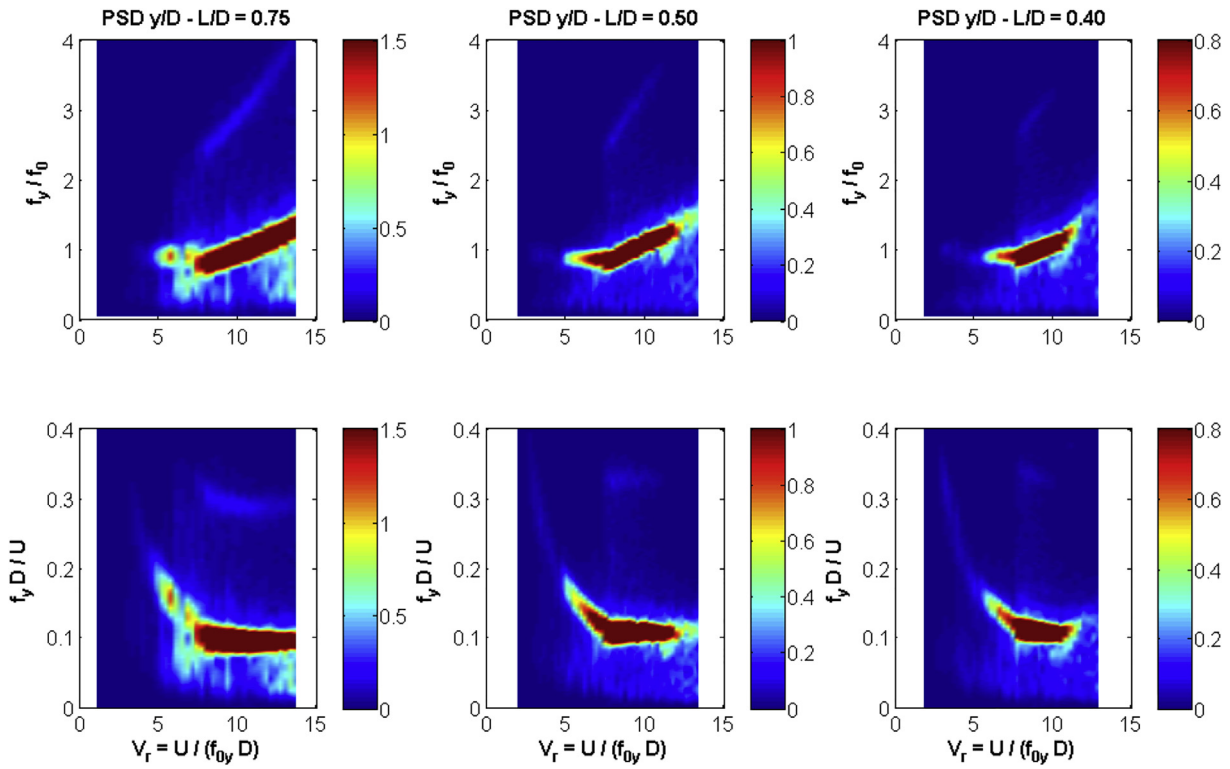

Fig. 13. PSD of the motion in the transverse direction as a function of $\mathbf{V_r}$ for cylinders with mass ratio of $\mathbf{m}^* = 1.00$ and different aspect ratios ($0.40 \leq \mathbf{L/D} \leq 0.75$).

metacentric height (GM) values are presented in Table 2.

The natural frequencies in still water in the in-line and transverse direction were practically the same for each L/D condition, $f_{0x}/f_{0y} \sim 0.97$; due to this, it is possible to consider $f_{0x} = f_{0y} = f_0$. The natural frequency in still water for the vertical direction, roll, pitch, and yaw were also calculated from decay tests. The damping coefficient in the transverse direction in still water was almost the same for all conditions, $\zeta_w \sim 4\%$. The structural damping was very low around $\zeta_s = 0.1\%$. All these results are presented in Table 3.

Forty velocity conditions were carried out for each aspect ratio. The reduced velocity range performed was $2 < V_r < 14$ and the Reynolds number range was $2 \times 10^3 < Re < 6 \times 10^4$, which corresponds to current incidences of $0.02 < U < 0.45$ m/s. The reduced velocity was calculated using the natural frequency in the still water in the transverse direction as $V_r = U/f_{0y}D$ or $V_r = U/f_0D$ as adopted.

The Froude number of the tests was defined as a function of the flow velocity and the cylinder submerged length as $\mathrm{Fr}_L = U/\sqrt{gL}$, as proposed by Chaplin and Teigen (2003). As can be seen in Table 4, only a few cases have $\mathrm{Fr}_L > 0.5$ for the highest reduced velocities. For these particular conditions, $L/D < 0.4$ and high velocities, the free-surface effects are significant and can introduce more tridimensional effects in the flow, but these effects could not be detached from the free-end effects.

Details about the conditions tested are presented in Table 4.

4. Analysis methodology

4.1. Characteristic amplitudes and frequencies

The values of characteristic amplitudes for each degree of freedom, as well as the characteristic frequencies, were obtained employing the Hilbert-Huang Transform Method (HHT) as proposed by Gonçalves et al. (2012a). The HHT was developed in Huang et al. (1998) as an alternative to deal with non-stationary signals that arise from non-linear systems. The characteristic amplitude was defined by taking the mean of the 10% largest amplitudes obtained in the HHT. It is important to highlight that in the HHT, there are instantaneous amplitudes of motion, which makes the number of points to calculate the mean of the 10% largest amplitudes proportional to the length of data and, consequently, to the sampling frequency, which implies a reduction in the statistic uncertainty. On the other hand, using the traditional 10% largest peak amplitudes, there are few points to evaluate the statistics as compared to the HHT. The characteristic motion frequency was defined by taking the frequency related to the 10% largest amplitudes obtained in the HHT.

The 6dof were measured during the tests. The modal form factor, as defined by Blevins (1990), utilized was $\gamma = 1$ to obtain the characteristic amplitudes due to the cylinder being considered a rigid body mounted on an elastic support. In sum, the modal form factor is a way of considering the characteristic of the natural vibration of the support structure, allowing displacements in any location to be accurately compared to the translational movement of a rigid structure, for instance, a cylinder elastically supported. This value will be significant in comparison with the results from the literature during the discussion of the results.

The PSD results were evaluated using the Fast Fourier Transform Method (FFT) and plotted in a color graph as a function of the reduced velocity.

4.2. Force coefficients

The linear rigid body motion equations for a cylinder with two uncoupled dof, in-line and transverse direction, are represented by the following equations proposed and discussed in Sarpkaya (2004) as shown below:

$$m_s\ddot{x}(t) + c\dot{x}(t) + k_x x(t) = F_{Hx}(t) \quad (1)$$

$$m_s\ddot{y}(t) + c\dot{y}(t) + k_y y(t) = F_{Hy}(t) \quad (2)$$

where m_s represents the cylinder mass; c the structural damping coefficient of the system; F_{Hx} and F_{Hy} are the total hydrodynamic forces acting

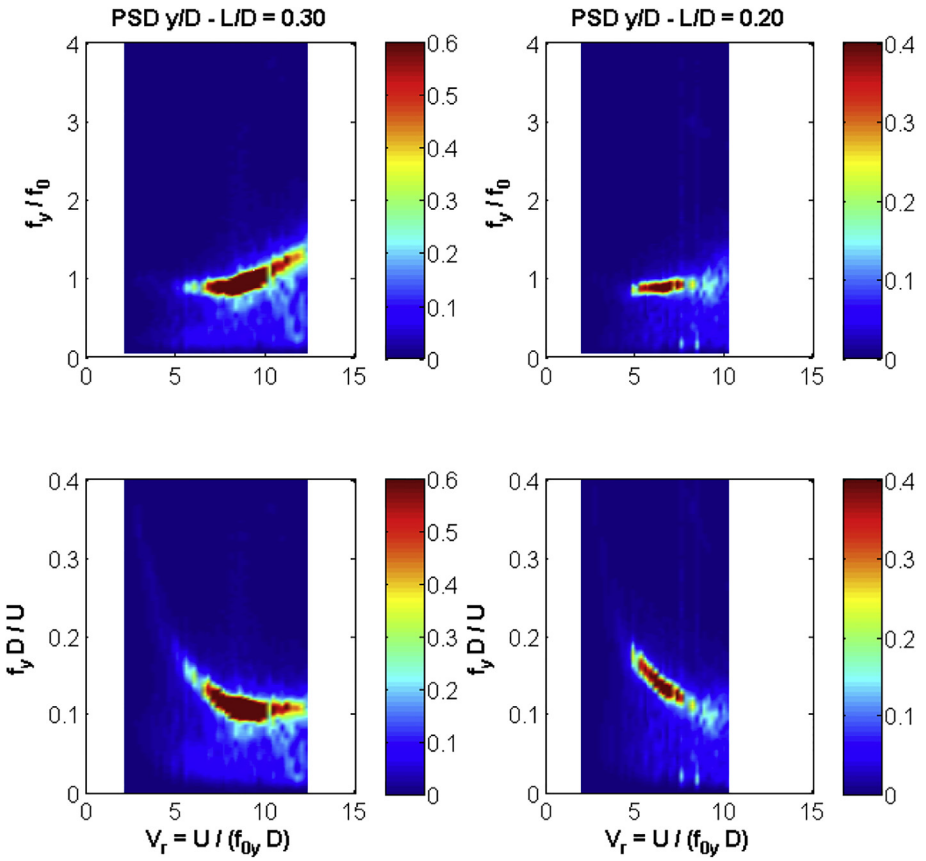

Fig. 14. PSD of the motion in the transverse direction as a function of $\mathbf{V_r}$ for cylinders with mass ratio of $\mathbf{m^* = 1.00}$ and different aspect ratios ($\mathbf{0.20 \leq L/D \leq 0.30}$).

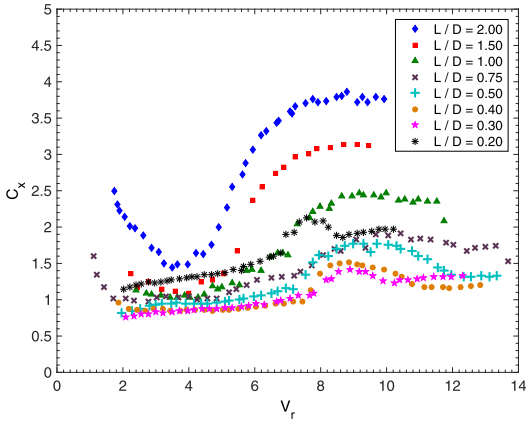

Fig. 15. Mean drag force coefficient ($\boldsymbol{C_x}$) as a function of reduced velocity ($\boldsymbol{V_r}$) for cylinders with mass ratio of $\boldsymbol{m^* = 1.00}$ and eight different aspect ratios ($\boldsymbol{L/D \leq 2.00}$).

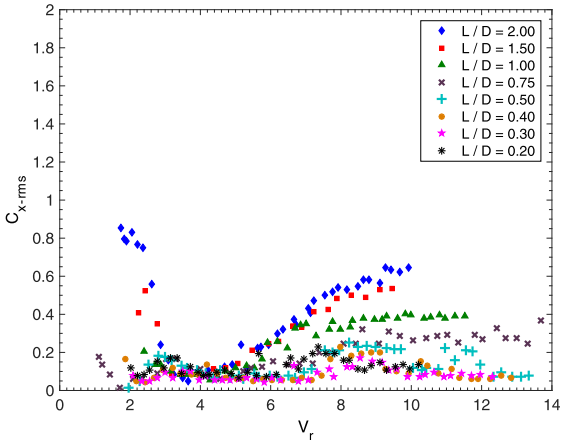

Fig. 16. Oscillatory drag force coefficient ($\boldsymbol{C_{x-rms}}$) as a function of reduced velocity ($\boldsymbol{V_r}$) for cylinders with mass ratio of $\boldsymbol{m^* = 1.00}$ and eight different aspect ratios ($\boldsymbol{L/D \leq 2.00}$).

on the system in the in-line, x, and transverse, y, directions. The structural damping ratio for the tests is $\zeta_s = 0.1\%$, which allows neglecting the structural damping force component.

In these equations, the 'structural' forces are placed on the left side; and the hydrodynamic forces, which include added mass (force component in phase with acceleration), hydrodynamic damping (force component in phase with velocity) and other forces due to fluid, are placed on the right side.

In the experiments, the total hydrodynamic forces in each given direction are measured indirectly using these motion equations. The total hydrodynamic force is the sum of the inertial, dissipative and restoring forces of the system (the restoring forces were derived from the position and stiffness values of each mooring spring), then the force is decomposed in the in-line and in the transverse direction.

The force in the transverse direction of the flow is commonly represented in the form of the nondimensional lift force coefficient, C_y, as in

$$F_{Hy}(t) = \frac{1}{2}\rho LDU^2 C_y(t) \tag{3}$$

$$C_y(t) = \frac{2F_{Hy}(t)}{\rho LDU^2} \tag{4}$$

where ρ is the fluid density.

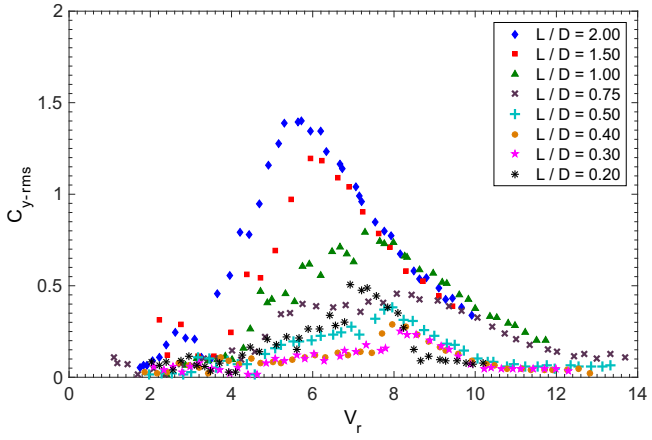

Fig. 17. Lift force coefficient (C_{y-rms}) as a function of reduced velocity (V_r) for cylinders with mass ratio of $m^* = 1.00$ and eight different aspect ratios ($L/D \leq 2.00$).

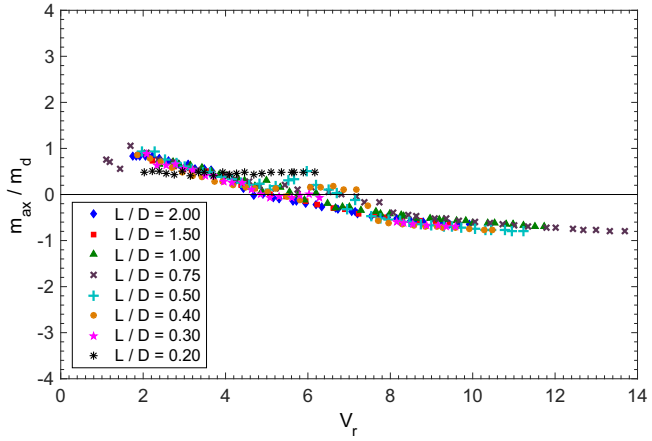

Fig. 18. Added mass coefficient in the in-line direction (m_{ax}/m_d) as a function of reduced velocity (V_r) for cylinders with mass ratio of $m^* = 1.00$ and eight different aspect ratios ($L/D \leq 2.00$).

The non-time dependent lift force coefficient, C_{y-rms}, was evaluated as the root mean square (RMS) of the non-dimensional force signal in the transverse direction.

The force in the in-line direction to the flow is commonly represented in the form of the nondimensional drag force coefficient, C_x, as in

$$F_{Hx}(t) = \frac{1}{2}\rho A_P U^2 C_x(t) \tag{5}$$

$$C_x(t) = \frac{2F_{Hx}(t)}{\rho LDU^2} \tag{6}$$

The force in the in-line direction can be divided into two components, one related to the average drag force (static component) and a second one related to the dynamic drag force (oscillatory component). Thus, the mean drag force can be described as $\overline{C_x}$, and the non-time dependent oscillatory drag force coefficient C_{x-rms} can be evaluated as the RMS of the non-dimensional force signal in the in-line direction.

4.3. Added mass coefficient

Considering, as usual, that the component of the total hydrodynamic force in phase with the acceleration is related to the added mass, it is possible to evaluate the added mass coefficient at the characteristic frequency of the motion, from a standard frequency domain analysis, as proposed by Fujarra and Pesce (2002). For the motions in the transverse direction:

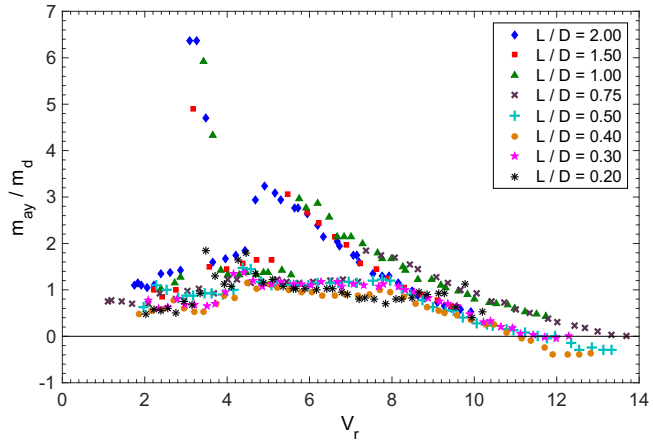

Fig. 19. Added mass coefficient in the transverse direction (m_{ay}/m_d) as a function of reduced velocity (V_r) for cylinders with mass ratio of $m^* = 1.00$ and eight different aspect ratios ($L/D \leq 2.00$).

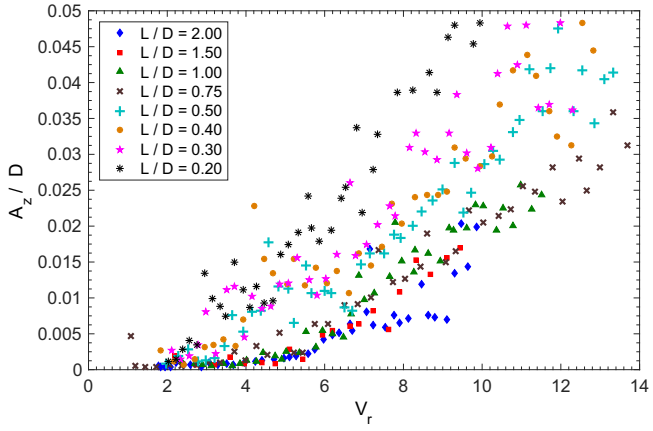

Fig. 20. Characteristic motion amplitude in the vertical direction (A_z/D) as a function of reduced velocity (V_r) for cylinders with mass ratio of $m^* = 1.00$ and eight different aspect ratios ($L/D \leq 2.00$).

$$m^*_{ay}(f_y) = -\mathscr{R}\left\{\frac{\frac{\mathscr{F}[F_{Hy}]}{\mathscr{F}[\ddot{y}]}}{m_d}\right\} \tag{7}$$

where $\mathscr{R}[]$ is the real part of the complex number and $\mathscr{F}[]$ is the fast Fourier transform operator. The same procedure is applied to the motions in the in-line direction.

5. Experimental results

The results from the experiments performed considering floating cylinders with very low aspect ratio are presented next, comprising characteristic amplitudes and frequencies in all the 6dof as a function of the reduced velocity, $V_r = U/f_0 D$, as well as the PSD for supporting the discussions and conclusions. Additionally, results of force coefficients and added mass are presented for the in-line and transverse directions.

Fig. 4 and Fig. 5, respectively, show the transverse, $A_y/(\gamma D)$, and in-line, $A_x/(\gamma D)$, characteristic amplitudes for the case of $m^* = 1$ and $L/D = 0.2, 0.3, 0.4, 0.5, 0.75, 1.0, 1.5$ and 2.0. In general, the amplitudes decrease with decreasing aspect ratio. The amplitude curves seem to shift

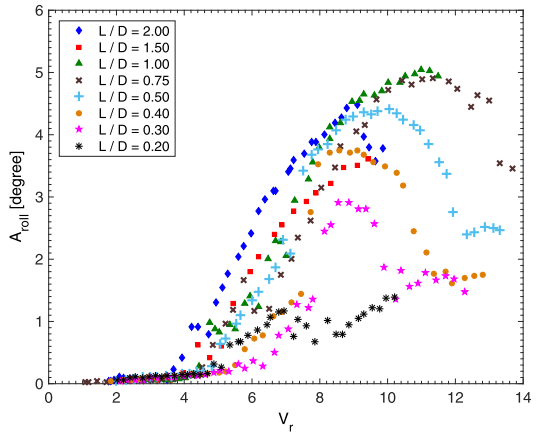

Fig. 21. Characteristic roll motion amplitude (A_{roll}) as a function of reduced velocity (V_r) for cylinders with mass ratio of $m^* = 1.00$ and eight different aspect ratios ($L/D \leq 2.00$).

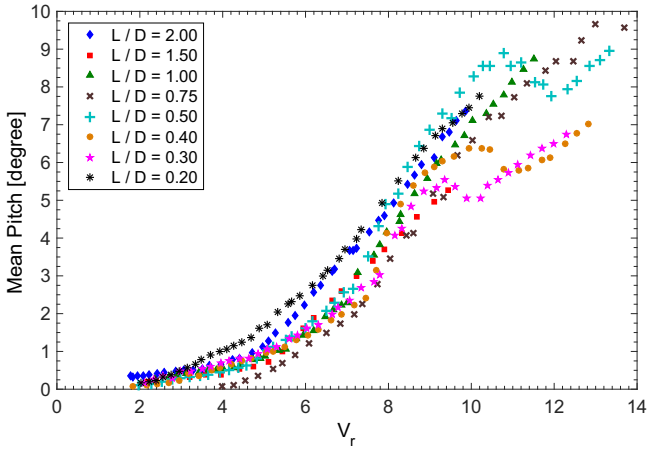

Fig. 23. Mean pitch angle as a function of reduced velocity (V_r) for cylinders with mass ratio of $m^* = 1.00$ and eight different aspect ratios ($L/D \leq 2.00$).

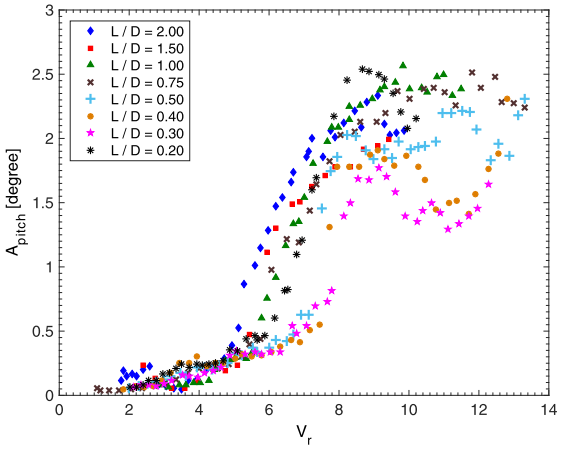

Fig. 22. Characteristic pitch motion amplitude (A_{pitch}) as a function of reduced velocity (V_r) for cylinders with mass ratio of $m^* = 1.00$ and eight different aspect ratios ($L/D \leq 2.00$).

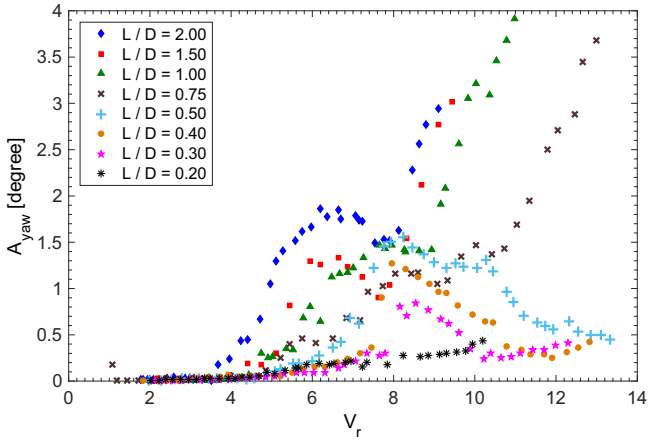

Fig. 24. Characteristic yaw motion amplitude (A_{yaw}) as a function of reduced velocity (V_r) for cylinders with mass ratio of $m^* = 1.00$ and eight different aspect ratios ($L/D \leq 2.00$).

to the right when the aspect ratio decreases. This fact can be associated with the free-end effects.

The characteristic amplitudes in the transverse direction, $A_y/(\gamma D)$, showed a distinct behavior for $L/D \geq 0.75$, see Fig. 4. In these cases, it was possible to observe a growth in amplitudes with increasing V_r, but it is not possible to see the amplitude fall, which is one characteristic of the *lower branch*. In the cases of $0.5 \leq L/D \leq 0.3$, the results showed a decrease of amplitudes for $V_r > 8$ and an abrupt fall for $V_r > 10$; the latter behavior can characterize the *lower branch*. On the other hand, for $L/D = 0.2$, the amplitudes in the transverse direction did not exceed $A_y/(\gamma D) = 0.2$, and there was no resonant behavior in this lowest aspect ratio. The maximum amplitudes are similar to $A_y/(\gamma D) \cong 1.4$ for $1 \leq L/D \leq 2$; the maximum values are $A_y/(\gamma D) \cong 1.1$ for $L/D = 0.75$; moreover, the maximum amplitudes vary around $0.6 < A_y/(\gamma D) < 0.8$ with higher amplitudes for larger aspect ratio for $0.3 \leq L/D \leq 0.5$.

The characteristic amplitudes in the in-line direction, $A_x/(\gamma D)$, also showed a distinct behavior for $L/D \geq 0.75$, see Fig. 5. In these cases, one first local maximum was found around $V_r \sim 3$, and it is possible to observe an abrupt growth for $V_r > 5$ with the maximum value around $V_r \sim 7$. In the cases of $0.2 \leq L/D \leq 0.5$, the results showed a linear increase of amplitudes for $V_r > 6$ and similar maximum values for this range of aspect ratio. The maximum amplitudes are $A_x/(\gamma D) \cong 0.45$ and $A_x/(\gamma D) \cong 0.25$ for $L/D = 2$ and $0.2 \leq L/D \leq 0.5$, respectively.

The results of the ratio between the transverse motion frequency and the natural transverse frequency in still water, f_y/f_0, presented in Fig. 6, showed the resonance behavior of the motion in the in-line direction for $2 < V_r < 4$ and $L/D \geq 1$. This response is characterized by $f_y \sim 0.5 f_0$ and $f_x \sim f_0$, thus $f_x/f_y \sim 2.0$. A linear increase of f_y/f_0 as a function of V_r occurred for $V_r > 4$ and $L/D \geq 1$. In this region, it is possible to assume that the vortex shedding frequency is similar to the motion frequency in the transverse direction, $f_s \cong f_y$, making it feasible to infer the Strouhal number as the curve inclination. Yet a constant value of $f_y/f_0 \sim 0.9$ up to $V_r \sim 7$ for $L/D \leq 0.75$ was observed; only after this reduced velocity did the linear increase of f_y/f_0 as a function of V_r occur.

The Strouhal "like" number can be evaluated considering the hypothesis that the frequency of the vortex shedding is similar to the frequency of the motion in the transverse direction in the synchronization range, i.e. $f_s \sim f_y$. The Strouhal "like" number was calculated as the inclination of the line in the graph of $f_y/f_0 \times V_r$ using linear fitting along the synchronization range. The results of the Strouhal like number for the cylinders with very low aspect ratio and 6dof are presented in Fig. 7. The present results were compared with the results from fixed tests performed in Gonçalves et al. (2015), VIV of low aspect ratio cylinders with 2dof by Gonçalves et al. (2013a), and results from cylinders with high aspect ratio. The Strouhal "like"number values, St, was obtained from linear fitting with $R^2 > 0.999$, which showed a large linear agreement between the data in the synchronization range.

In the Strouhal "like" number results in Fig. 7 the St was observed to

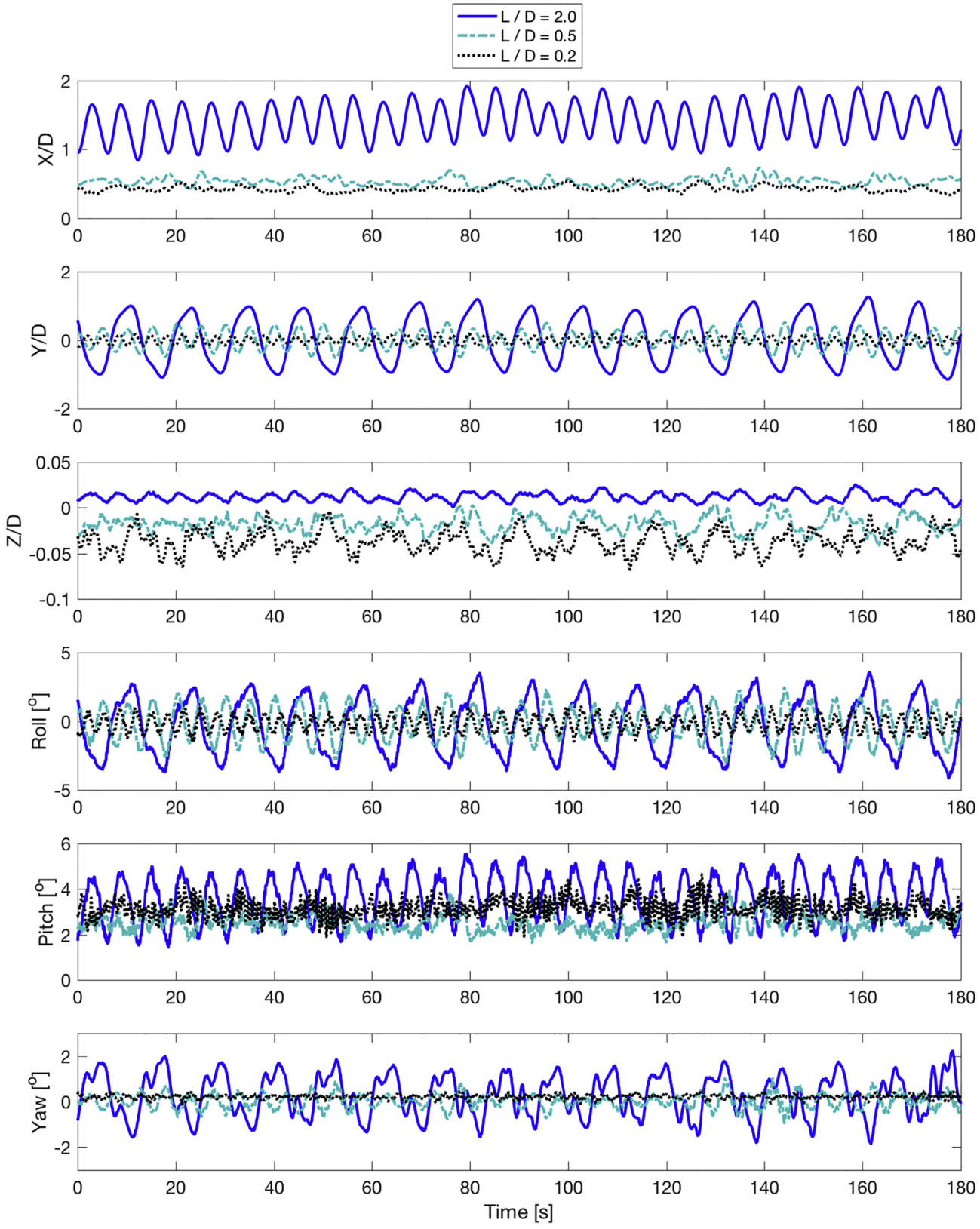

Fig. 25. Example of time series of the 6dof motions at $V_r \sim 7$ for the cylinders with mass ratio of $\mathbf{m}^* = 1.00$ and $\mathbf{L/D} = 2.0$, 0.5 and 0.2.

decrease with the decrease of the aspect ratio for cylinders with 2dof in the range $1.5 \leq L/D \leq 2.0$. The same behavior occurred for the cylinders with 6dof in two different ranges namely $1.0 \leq L/D \leq 2.0$ and $0.3 \leq L/D \leq 0.5$. It is possible to conjecture that in the first range, $1.0 \leq L/D \leq 2.0$, the von Kármán was still present, and it was governing the motion; on the other hand, in the second range, $0.3 \leq L/D \leq 0.5$, the von Kármán was not presented, and the resonance motion was governed by the structures shedding around the cylinder free end. All the values

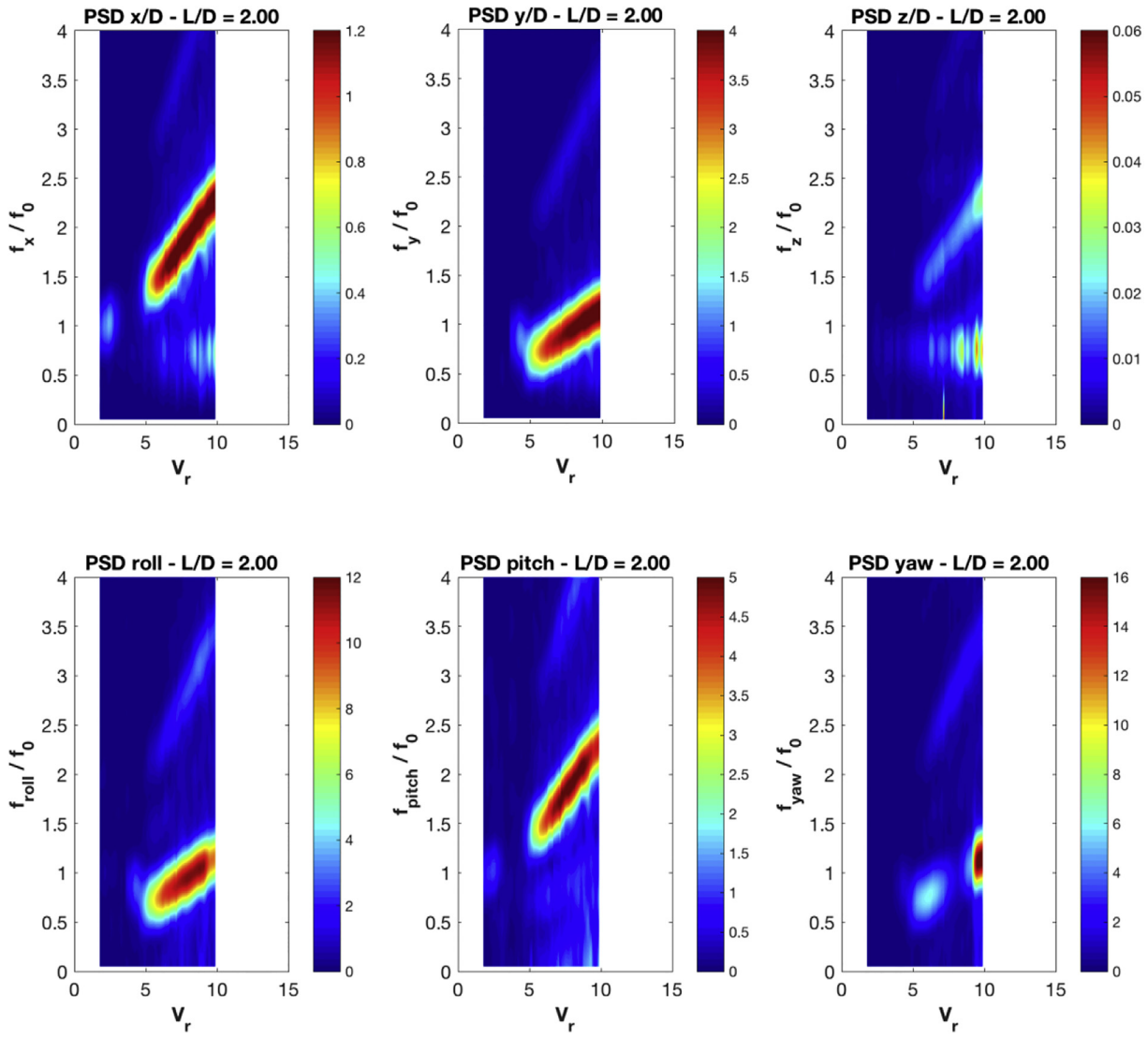

Fig. 26. PSD of the 6dof motions as a function of $\mathbf{V_r}$ for the cylinder with mass ratio of $\mathbf{m^*} = 1.00$ and $\mathbf{L/D} = 2.0$.

were lower than the values for the cylinders with high aspect ratio, $L/D > 13$.

The decrease in the Strouhal number due to the decrease in the aspect ratio was also observed for the fixed tests as presented by Okamoto and Yagita (1973), Sakamoto and Arie (1983), Fox and Apelt (1993), Norberg (1994) and Gonçalves et al. (2015). Significant result, highlighted for cylinders with high aspect ratio by Leong and Wei (2008) and Stappenbelt and Lalji (2008), is that the Strouhal number verified for cylinders under VIV, $St \cong 0.16$, is lower than the one verified for the fixed cases, $St \cong 0.20$, as presented in Williamson and Govardhan (2004). The same behavior was observed for the present results for cylinders with very low aspect ratio.

Examining the last results presented together with the results of the ratio between in-line and transverse motion frequencies, f_x/f_y, see Fig. 8, the reduced velocity range in which the linear behavior of f_y/f_0 was observed seems to be the same as the couple between the motions in the in-line and in the transverse direction occurred, a region characterized by $f_x/f_y \cong 2$. For $L/D \leq 0.5$, it was possible to observe values of $f_x/f_y \leq 0.5$ in high values of reduced velocities; these reduced velocities were the same as the abrupt fall of the amplitudes in the transverse direction, confirming the existence of the *lower branch* and the loss of synchronism of the shedding frequency and the motion frequency of the cylinder. The case of $L/D = 0.2$ was different because it did not present the coupled behavior $f_x/f_y \cong 2$ in any reduced velocity condition. This result, together with the amplitude results, confirms that the typical VIV behavior was not observed for $L/D = 0.2$, i.e., there was no vortex shedding capable of synchronizing the frequency of the cylinder motion, and the structures formed around this aspect ratio were not capable of creating alternating forces and, consequently, motion in the cylinder. The same behavior was observed for stationary cylinders with low aspect ratio presented in Gonçalves et al. (2015); in that work, the value of $L/D = 0.2$ showed to be critical concerning alternating forces generation.

The PSD results of the motions in the in-line and in the transverse directions as a function of reduced velocities for each aspect ratio are presented in Figs. 9–14 to corroborate the statements made so far.

The PSD results of the motions in the in-line direction, see Figs. 9–11, showed the region where the dominant in-line frequency is defined. This region is characterized by an inclined line when looking at the graph of f_x/f_0 as a function of V_r, and also by a line with constant value when looking at the graph of f_xD/U as a function of V_r. The range of these lines was observed to decrease with decreasing aspect ratio, and this line did not exist for $L/D = 0.2$. For $L/D \leq 0.5$. A second region with considerable energy density was observed for $V_r > 7$, with lower dominant frequencies around $f_x/f_0 \sim 0.4$.

The PSD results of the motions in the transverse direction, see Figs. 12–14, showed the region where the dominant transverse frequency

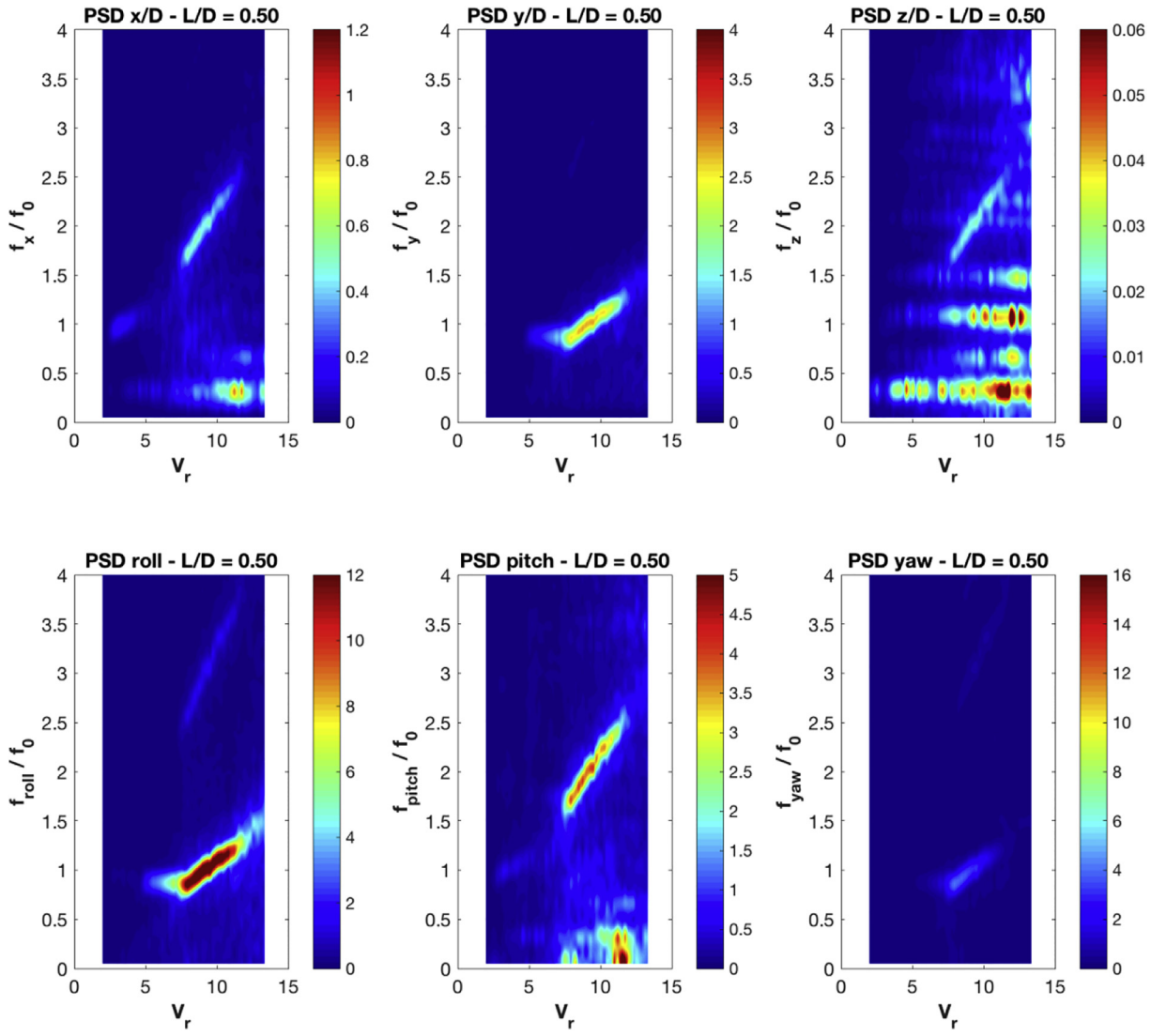

Fig. 27. PSD of the 6dof motions as a function of $\mathbf{V_r}$ for the cylinder with mass ratio of $\mathbf{m^*} = 1.00$ and $\mathbf{L/D} = 0.5$.

is defined. This region is also characterized by an inclined line, practically with half the inclination verified in the in-line direction, when looking at the graph of f_x/f_0 as a function of V_r; and also by a line with constant value, practically half that verified in the in-line direction, when looking at the graph of f_xD/U as a function of V_r. These values characterize the Strouhal number for each aspect ratio condition assuming that the vortex shedding frequency is similar to the motion frequency in the transverse direction, $f_s \cong f_y$.

In the same way as the in-line direction, the range of these lines was observed to decrease with decreasing aspect ratio. For $L/D = 0.2$, the positive inclination of the line was not found and the value was constant $f_y/f_0 \sim 1$. For $L/D \leq 0.5$, a previous region before the inclined line was observed where the value is constant $f_y/f_0 \sim 1$, which showed a different behavior when compared with the higher aspect ratios.

It is interesting to draw a parallel between the PSD results of the cylinder free to oscillate with 6dof, see Figs. 9–14, with the PSD results of the stationary cylinder obtained by Gonçalves et al. (2015). In those results, a different behavior was observed for stationary cylinders with $L/D \leq 0.5$; in those cases, the cylinder free end was responsible for changing the structures shedding around the cylinder, and these structures were responsible for the considerable energy density in lower frequencies. In those cases, the typical von Karmán street was not verified. For $L/D \leq 0.2$, alternating forces were not observed. The same behaviors were verified and confirmed for the cylinders free to oscillate with 6dof, showing the coherence between the results and confirming the statements made before.

The results of mean drag force coefficient, $\overline{C_x}$, and oscillatory drag force coefficient, C_{x-rms}, are presented in Fig. 15 and Fig. 16, respectively. The results of drag coefficient showed to be similar to that presented for characteristic amplitudes, i.e. the drag force coefficient decreased with decreasing aspect ratio, see Fig. 15. The mean drag force coefficient results allow observing the dynamic drag amplification behavior when $f_x/f_y \cong 2$, except for $L/D = 0.2$. The force characteristics were different for $L/D = 0.2$; the same behavior was presented by Gonçalves et al. (2015) for fixed cylinders and $L/D = 0.2$ due to the combined presence of free-end and free-surface effects. The maximum values of mean drag coefficient reach $\overline{C_x} \cong 4$ and $\overline{C_x} \cong 1.5$, respectively, for $L/D = 2.0$ and $L/D = 0.5$.

The results of oscillatory drag force coefficient, C_{x-rms}, showed high values in the region of in-line resonance for $V_r < 4$ and $L/D > 0.5$. For $L/D < 0.5$, the $C_{x-rms} \cong 0.2$ is almost constant and lower than for the highest aspect ratio. It is possible to see for these aspect ratios, $L/D < 0.5$, that the in-line amplitudes were also low. The maximum values of oscillatory drag coefficient reach $C_{x-rms} \cong 0.9$ and $C_{x-rms} \cong 0.3$, respectively, for $L/D = 2.0$ and $L/D = 0.5$.

The results of lift force coefficient, C_{y-rms}, are presented in Fig. 17.

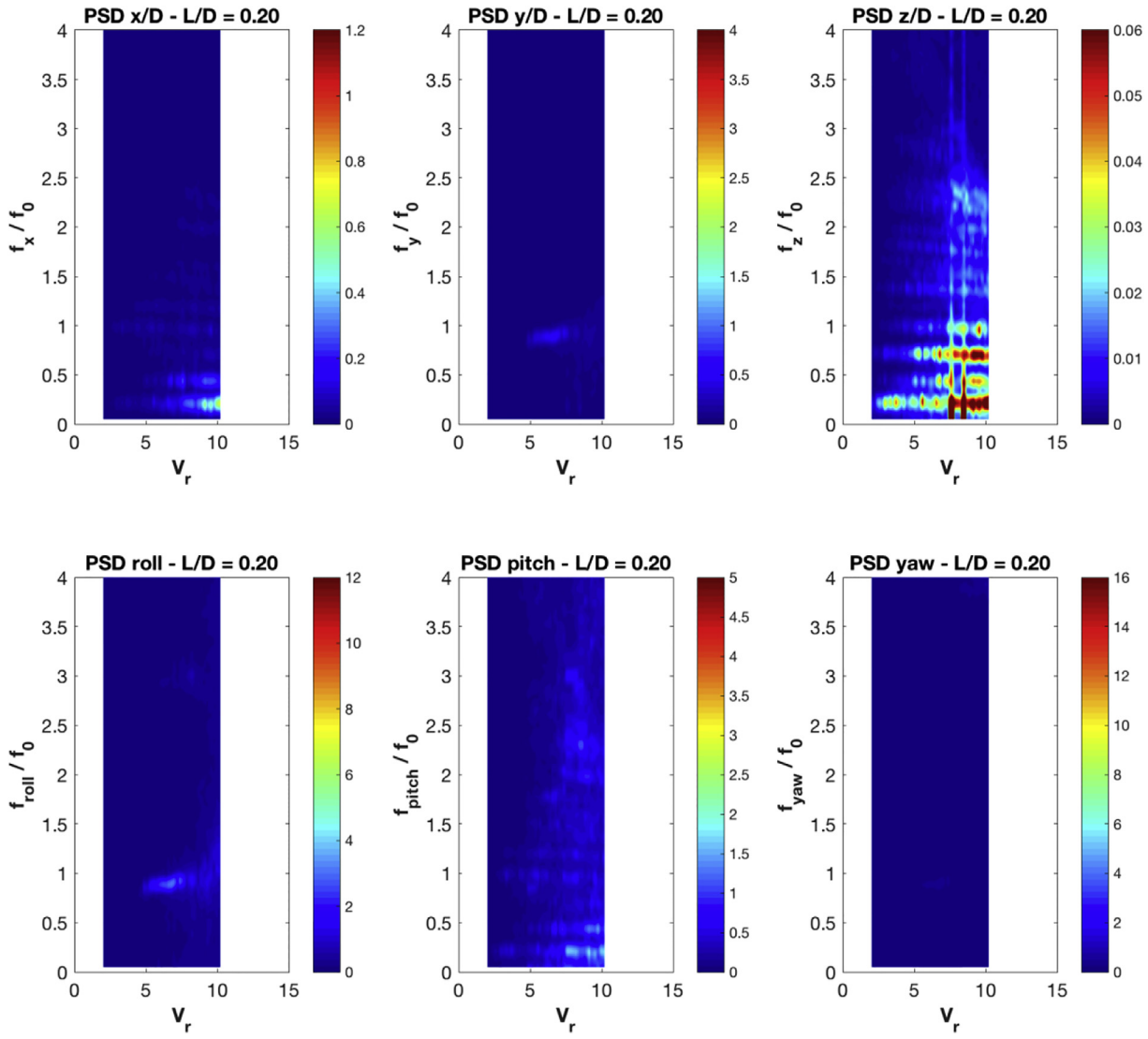

Fig. 28. PSD of the 6dof motions as a function of $\mathbf{V_r}$ for the cylinder with mass ratio of $\mathbf{m^*} = 1.00$ and $\mathbf{L/D} = 0.2$.

The results of lift force coefficient also decreased with decreasing aspect ratio. For $L/D \geq 1.00$, it was possible to observe two local maxima, the first one related to the in-line resonance in $V_r \cong 3$ and the second one related to the beginning of the synchronization process between in-line and transverse motions. The results of lift force coefficient showed that the maximum value of C_{y-rms} occurred at lower reduced velocity with increasing aspect ratio. The maximum values of lift force coefficient reach $C_{y-rms} \cong 1.4$ and $C_{y-rms} \cong 0.4$, respectively, for $L/D = 2.0$ and $L/D = 0.5$.

The added mass results for the in-line direction, in Fig. 18, showed a decrease with increasing reduced velocity with an asymptotic value of $m^*_{ax} = -1$, the same behavior reported in Jauvtis and Williamson (2004) and in Cunha et al. (2006). The zero crossing occurred for all cases around $V_r \approx 4$, which confirms the resonance of the in-line motion around this reduced velocity, except for $L/D = 0.2$; in the latter case, the VIV behavior was not observed.

However, the added mass results for the transverse direction, Fig. 19, did not present the zero crossing regions, confirming the absence of the lower branch for $L/D > 0.5$ and $V_r < 14$. In turn, added mass results for high aspect ratio cylinders, as in Vikestad et al. (2000), usually show a zero crossing where the lower branch appears, and the resonant process is finished. In fact, for $0.2 < L/D \leq 0.5$, the curve crossed zero confirming the presence of *lower branch* for these cases besides pointing out the characteristic amplitudes in the transverse direction presented in Fig. 4.

The characteristic amplitudes in the vertical direction, A_z/D, presented larger amplitudes for lower aspect ratio and also an increase in the amplitudes by increasing the reduced velocity, see Fig. 20. The vertical amplitudes are related to wave generation on the free surface, i.e. the vertical amplitudes depend on the Froude number, Fr_L. However, the vertical amplitudes are very low $A_z/D < 0.05$, and their effects on the VIM can be neglected.

The characteristic roll, A_{roll}, and pitch A_{pitch}, motion amplitudes are presented in Fig. 21 and Fig. 22, respectively. The roll motions were coupled directly to the motions in the transverse direction for $V_r < 8$, and coupled to the motion in the transverse direction and yaw motion for $V_r > 8$. As can be seen in Fig. 24, the yaw motion presented local minima around $V_r = 8$ for $L/D > 0.5$, and the yaw amplitudes increased suddenly after this reduced velocity. It is interesting to note that the natural frequency of yaw motion was higher than the transverse one and the yaw could be resonant for larger reduced velocities, but the reduced velocities tested were not enough to verify this behavior.

The maximum characteristic roll motion amplitude was $A_{roll} \cong 5$ for the cases with highest aspect ratio, and the trend was a decrease in the roll motion amplitudes with a decrease in the aspect ratio, see Fig. 21. Moreover, the maximum characteristic pitch amplitude was $A_{pitch} \cong 2.5$, see Fig. 22. The value for the maximum characteristic pitch amplitude

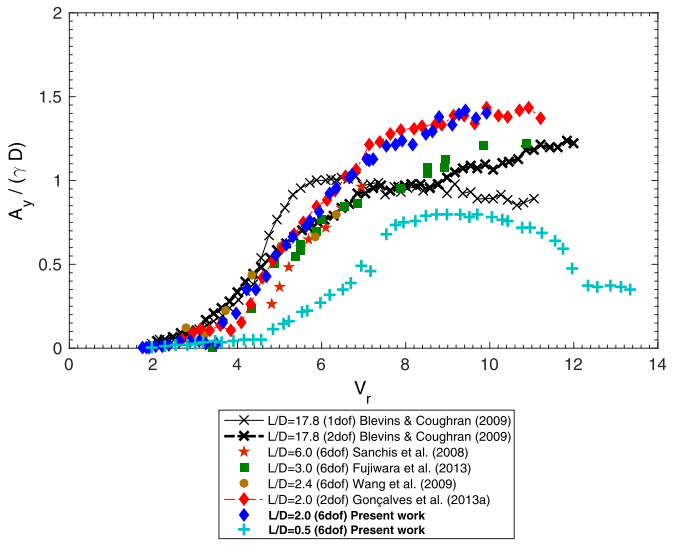

Fig. 29. Literature comparison of the characteristic motion amplitude in the transverse direction ($A_y/(\gamma D)$) as a function of reduced velocity (V_r) for cylinders with the mass ratio of $m^* = 1.00$.

Table 5
Works about VIV of circular cylinders with $m^* = 1.00$ for the comparison.

Work	L/D	m^*	dof	V_r
Blevins and Coughran (2009)	17.8	1.00	1	2 → 12
	17.8	1.00	2	2 → 12
Sanchis et al. (2008)	6.0	1.00	6	4 → 7
Fujiwara et al. (2013)	3.0	1.00	6	3 → 11
Wang et al. (2009)	2.4	1.00	6	2 → 7
Gonçalves et al. (2013a)	2.0	1.00	2	2 → 12
Present work	2.0	1.00	6	2 → 10
	0.5	1.00	6	2 → 14

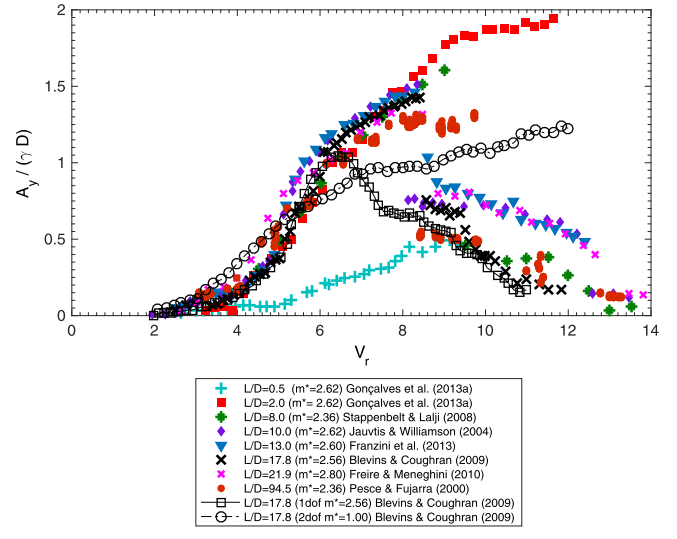

Fig. 30. Literature comparison of the characteristic motion amplitude in the transverse direction ($A_y/(\gamma D)$) as a function of reduced velocity (V_r) for cylinders with the mass ratio around $m^* \sim 2.5$ and 2dof.

was lower than the roll ones also seeing that the amplitudes in the in-line direction were lower than the transverse one. The trend was the same for the roll motion amplitudes except for the $L/D = 0.2$, in which the pitch motion amplitudes were higher than the higher aspect ratio cases. This behavior can be attributed to the free surface effect in this case due to

Table 6
Works about VIV of circular cylinders with $m^* \cong 2.50$ for the comparison.

Work	L/D	m^*	dof	V_r
Pesce and Fujarra (2000)	94.5	2.60	2	2 → 11
Freire and Meneghini (2010)	21.9	2.80	2	2 → 10
Blevins and Coughran (2009)	17.8	2.56	1	2 → 11
	17.8	2.56	2	2 → 12
	17.8	1.00	2	2 → 12
Franzini et al. (2013)	13.0	2.60	2	2 → 13
Jauvtis and Williamson (2004)	10.0	2.62	2	2 → 14
Stappenbelt and Lalji (2008)	8.0	2.36	2	2 → 14
Gonçalves et al. (2013a)	2.0	2.62	2	2 → 12
	0.5	2.62	2	2 → 10

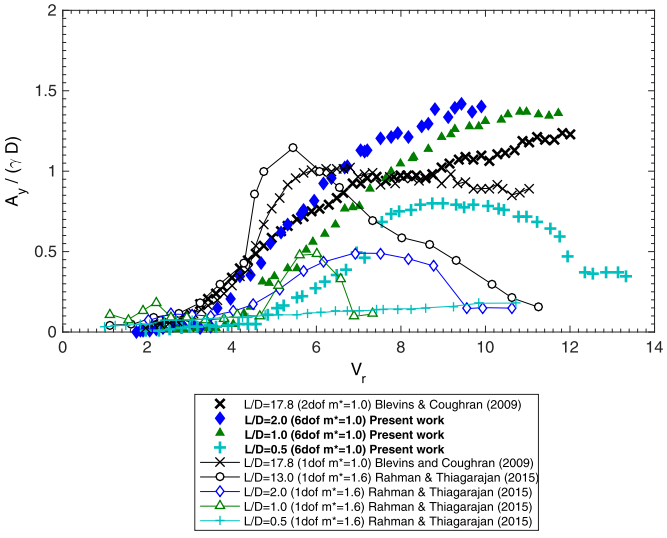

Fig. 31. Literature comparison of the characteristic motion amplitude in the transverse direction ($A_y/(\gamma D)$) as a function of reduced velocity (V_r) for cylinders with very low aspect ratio and small mass ratio.

Table 7
Works about VIV of circular cylinders with very low aspect ratio and small mass ratio.

Work	L/D	m^*	dof	V_r
Blevins and Coughran (2009)	17.8	1.00	1	2 → 11
	17.8	1.00	2	2 → 12
Rahman & Thiagarajan (2015)	13.0	1.60	1	1 → 12
	2.0	1.60	1	2 → 11
	1.0	1.60	1	1 → 8
	0.5	1.60	1	2 → 11
Present work	2.0	1.00	6	2 → 10
	1.0	1.00	6	2 → 12
	0.5	1.00	6	2 → 14

$Fr_L > 0.5$.

The mean pitch angle results are presented in Fig. 23. For all aspect ratio cases, the mean pitch angle is similar and increased by increasing the reduced velocity. Distinct behavior occurred at the start of the lower branch region for $0.2 < L/D \leq 0.5$; a decline in the amplitude was verified in this region, and the dynamic amplification of the drag ceased. In fact, results presented by Franzini et al. (2013) showed that angle values inferior to 10° do not substantially affect the VIV response for cylinders with $L/D = 13$. Therefore, the effect of the inclination can be neglected for the low aspect ratio cylinders presented here.

The characteristic yaw motion amplitudes, A_{yaw}, showed a large relation to the motions in the transverse direction, see Fig. 24. For the cases $L/D > 0.5$, it is possible to observe local minima in the same reduced velocity as the maximum lift coefficient occurred, and after this value increased in the yaw amplitudes A decrease in the yaw motion in

the highest reduced velocities tested for these cases was not observed. However, a drop was verified in the yaw amplitudes for the $L/D \leq 0.5$ in the same region characterized by the lower branch in the motions in the transverse direction. No yaw amplitudes higher than $A_{yaw} = 0.5$ were observed for $L/D = 0.2$. For the yaw motions, as well as for the motions in the transverse direction, it is possible to distinguish three different region behaviors, namely $0.5 < L/D \leq 2.0$, $0.2 < L/D \leq 0.5$ and $L/D = 0.2$.

Fig. 25 presents an example of the time series for all the 6dof at $V_r \sim 7$ for one case in each distinct behavior region commented before, namely $L/D =$ 2.0, 0.5 and 0.2. The couple between the different degrees of freedom is due to the elastically supported system applied to the experiments. It is possible to observe at the moment that the cylinder promoted motions in the transverse direction, the roll motion is coupled and in the same phase; the same occurred for the motions in the in-line direction and pitch motion.

The example time series shown in Fig. 25 helps to summarize the characteristic behavior for each region as: for the range $0.5 < L/D \leq 2.0$, von Kárman street main characteristic is predominant and the double frequency can be observed for motion in the in-line direction when compared with the frequency for motion to the transverse direction; for the $0.2 < L/D \leq 0.5$, even without von Kármán street main characteristics around the majority span length of the cylinder, the vortex shedding around it was capable of producing alternating forces in the transverse direction and no more double frequency in the motions in the in-line direction is observed; finally, for $L/D \leq 0.2$, low amplitudes are found in the transverse and in-line direction, and the free surface effects play an important role increasing the motions in the vertical direction and pitch motions; therefore, the vortex structure are not enough to produce significant VIV amplitudes.

The PSD results for all the 6dof presented in Fig. 26, Fig. 27 and Fig. 28 for $L/D =$ 2.0, 0.5 and 0.2, respectively, concerning frequency results corroborated the summary statement made before. The couple between the motion in the transverse direction and roll, as well as the couple between the motion in the in-line direction and pitch, can be highlighted, i.e. each pair of the degree of freedom presented the same frequency behavior. The results for L/D = 0.2 showed an absence of significant energy for most degrees of freedom. However, the increase of the energy for the motions in the vertical direction for low frequencies due to the increase in the free surface effects were also observed for this very low aspect ratio. Note that the vertical energy is not enough to change the VIV behavior for the motions in the transverse and in the in-line direction.

The analysis performed so far confirmed that the free-end effects increase with decreasing aspect ratio, mainly for $0.2 < L/D \leq 0.5$. In this range of aspect ratio, the structures formed around the cylinder free end are the only ones responsible for the alternating forces in the transverse direction, differently from the typical von Kármán street presented for higher aspect ratios.

6. Literature comparison

As detailed in the Introduction section of this work, few works in the literature are found about VIV of circular cylinders with low aspect ratio and small mass ratio. The goals of the present section are to compare the current results with the ones found in the literature and to show the consistency of our results.

Fig. 29 presents the literature comparison of the characteristic motion amplitude in the transverse direction for cylinders with the mass ratio of $m^* = 1.00$; details about the works compared are presented in Table 5. The first point to be detached is the difference between 1dof and 2dof results for $L/D = 17.8$, which confirms that the presence of the motions both in the in-line and in the transverse direction directly impact the VIV; on the other hand, 2dof and 6dof results $L/D = 2.0$ are similar, and this difference of degrees of freedom does not play an important role. The second one is the highest amplitudes occurring for $L/D = 2.0$ instead of the highest aspect ratio $L/D = 17.8$; as discussed in Gonçalves et al. (2013a, 2015) and confirmed by the present work, the low-frequency forces due to the free-end presence keep the synchronization for a longer time. In the latter, the results for $2.4 \leq L/D \leq 17.8$ are similar; therefore, the effect of the free-end presence may not affect the VIV behavior for $L/D \geq 2.4$. The amplitude results for $L/D = 0.5$ is the lowest due to the existence of the free-end structures for this case instead of the typical von Kármán street behavior for $L/D > 0.5$ as discussed in the Experimental Results section of this work.

Fig. 30 presents the literature comparison of the characteristic motion amplitude in the transverse direction for cylinders with the mass ratio of $m^* \sim 2.50$ and 2dof; details about the works compared are presented in Table 6. The results for $L/D = 17.8$ confirmed the difference between 1dof and 2dof for $m^* \sim 2.50$; also, it is possible to observe the difference between the results for and $m^* \sim 2.50$, statement discussed intensely in Jauvtis and Williamson (2004) for $L/D = 10$, and Gonçalves et al. (2013a) for low aspect ratio cylinders. Even for $m^* \sim 2.50$, the results for $L/D = 2.0$ presented higher amplitudes for $V_r > 8$ than cylinders with high aspect ratio cylinders. The explanation for the absence of the lower branch for the $V_r > 8$ may be the presence of low-frequency forces due to the free-end presence as commented before. As expected for the $L/D = 0.5$, the amplitudes are the lowest.

Fig. 31 presents the literature comparison of the characteristic motion amplitude in the transverse direction for cylinders with very low aspect ratio and small mass ratio, details about the works compared are presented in Table 7. Only the work by Rahman & Thiagarajan (2015) presented experimental results from VIV of $L/D \leq 2.0$. The results cannot be compared directly with the results of the current work because of the difference between mass ratio and degrees of freedom. Yet the conclusion is similar: the amplitudes in the transverse direction decrease when the aspect ratio decreases.

The literature review and comparison summed up the importance of having studied the floating cylinders with very low aspect ratio and have helped to fill this lack of studies.

7. Conclusion

The present work was motivated by the VIM studies on circular platforms, particularly the case of the monocolumn platform ($0.20 < L/D < 0.50$). It aimed to understand the VIV around floating circular cylinders with very low aspect ratio.

Hence, VIV experiments were carried out in a circulating water channel at NDF, Brazil. Eight different aspect ratio conditions were tested. In all the conditions, the cylinder was free to oscillate with 6dof and $m^* = 1$. Motions were acquired using an optical motion capture system. Results regarding motion amplitudes, motion characteristic frequencies, lift and drag forces and added mass were presented and discussed for each aspect ratio. Literature review and comparison were performed to corroborate the statements in this work.

Regarding the motion amplitudes, the characteristic amplitudes in both in-line and transverse directions decreased with decreasing aspect ratio. The results of drag and lift forces also showed the same behavior, confirming the reduction in amplitudes with decreasing aspect ratio. The same behavior was verified for the Strouhal number assuming that $f_y \cong f_s$. On the other hand, the added mass results helped to confirm the end of the resonant process when this value reached a value equal zero, and also for motions in the transverse direction to confirm the *lower branch* behavior. The motion amplitudes for the vertical direction, roll, pitch and yaw did not show to affect the VIV behavior since the energy of these degrees of freedom was low and related to the couple with the motions in the in-line and transverse direction.

Distinct responses were observed regarding the possible source of the alternating forces analyzing the characteristic frequency results: the first one, for cylinders with $0.5 < L/D \leq 2.00$, in which the von Kármán street

is present together with the structures formed around the cylinder free end; the second one, for cylinders with $0.20 < L/D \leq 0.50$, in which only the vortex formed and shedding around the cylinder free end were responsible for the resonant behavior of the system; and the last one, for cylinders with $L/D \leq 0.20$, in which the vortex structures due to the cylinder free end were predominant but not capable of promoting a VIV resonant behavior of the system; thus, the value $L/D = 0.20$ can be considered the critical aspect ratio value for the existence of VIV on cylinders.

These conclusions are similar those obtained for stationary cylinders with low aspect ratio and presented in previous work by Gonçalves et al. (2013a). These two works together can help to better understand the VIV behavior of low aspect ratio cylinders.

Future works can use CFD simulations to better visualize the structures formed around the cylinder free end and can further explain the phenomenon of flow around low aspect ratio cylinders.

Acknowledgements

The authors thank Rodrigo S. Campos for his help in performing the tests. The authors would also like to acknowledge the São Paulo Research Foundation (FAPESP), process number 2014/02043-1, and the Brazilian National Council for Scientific and Technological Development (CNPq) for supporting an important part of their VIV research at USP.

References

Antony, A., Parambath, A., Yue, B., Man, K., Thethi, R., 2017. Cost savings associated with improved VIM prediction accuracy. In: Proceedings of the Offshore Technology Conference, OTC-27889-MS. Houston, TX, USA.

Assi, G.R.S., 2005. Experimental Study of the Flow Interference Effect Around Aligned Cylinders. Master's thesis. University of São Paulo, São Paulo, Brazil (in Portuguese).

Bearman, P.W., 1984. Vortex shedding from oscillating bluff bodies. Annu. Rev. Fluid Mech. 16, 195–222.

Blevins, R.D., 1990. Flow-induced Vibration. Krieger, Malabar, FL.

Blevins, R.D., Coughran, C.S., 2009. Experimental investigation of vortex-induced vibration in one and two dimensions with variable mass, damping, and Reynolds number. J. Fluid Eng. 131, 101202–101207.

Chaplin, J.R., Teigen, P., 2003. Steady flow past a vertical surface-piercing circular cylinder. J. Fluid Struct. 18, 271–285.

Cunha, L.D., Pesce, C.P., Wanderley, J.B.V., Fujarra, A.L.C., 2006. The robustness of the added mass in VIV models. In: Proceedings of the 25th International Conference on Offshore Mechanics and Arctic Engineering, OMAE2006–92323. Hamburg, Germany.

Dijk, R.R., Magee, A., Perryman, S., Gebara, J., 2003. Model test experience on vortex induced vibrations of truss spars. In: Proceedings of the Offshore Technology Conference, OTC-15242. Houston, USA.

Finn, L.D., Maher, J.V., Gupta, H., 2013. The cell spar and vortex induced vibrations. In: Proceedings of the Offshore Technology Conference, OTC2003-15244. Houston, USA.

Fox, T.A., Apelt, C.J., 1993. Fluid-induced loading of cantilevered circular cylinders in a low-turbulence uniform flow, Part 3: fluctuating loads with aspect ratios 4 to 25. J. Fluid Struct. 7 (4), 375–386.

Franzini, G.R., Gonçalves, R.T., Meneghini, J.R., Fujarra, A.L.C., 2013. One and two degrees-of-freedom vortex-induced vibration experiments with yawed cylinders. J. Fluid Struct. 42, 401–420.

Freire, C.M., Meneghini, J.R., 2010. Experimental investigation of VIV on a circular cylinder mounted on an articulated elastic base with two degrees-of-freedom. In: Symposium on Bluff Body Wakes and Vortex-induced Vibrations, BBVIV6. Capri Island, Italy.

Fujarra, A.L.C., Pesce, C.P., 2002. Added mass of an elastically mounted cylinder in water subjected to vortex-induced vibrations. In: Proceedings of the 21st International Conference on Offshore Mechanics and Arctic Engineering, OMAE2002-28375. Oslo, Norway.

Fujiwara, T., Saito, M., Maeda, K., Sato, H., Ishida, K., 2013. Experimental investigation of VIM characteristics on column type floater in super critical Reynolds number. In: Proceedings of the 32nd International Conference on Ocean, Offshore and Arctic Engineering, OMAE2013–10473. Nantes, France.

Fukuoka, H., Hirabayashi, S., Suzuki, H., 2016. The effects of free surface and end cell on flow around a finite circular cylinder with low aspect ratio. J. Mar. Sci. Technol. 21 (1), 145–153.

Gonçalves, R.T., Rosetti, G.F., Fujarra, A.L.C., Nishimoto, K., 2010. Mitigation of vortex-induced motion (VIM) on a monocolumn platform: forces and movements. J. Offshore Mech. Arctic Eng. 132, pp. 041102-1-16.

Gonçalves, R.T., Franzini, G.R., Rosetti, G.F., Fujarra, A.L.C., Nishimoto, K., 2012a. Analysis methodology for vortex-induced motion (VIM) on a monocolumn platform applying the Hilbert-Huang transform method. J. Offshore Mech. Arctic Eng. 134 (1), 011103.

Gonçalves, R.T., Rosetti, G.F., Fujarra, A.L.C., Franzini, G.R., Freire, C.M., Meneghini, J.R., 2012b. Experimental comparison of two degrees-of-freedom vortex-induced vibration on high and low aspect ratio cylinders with small mass ratio. J. Vib. Acoust. 134, pp. 061009-1-7.

Gonçalves, R.T., Rosetti, G.F., Fujarra, A.L.C., Oliveira, A.C., 2012c. Experimental study on vortex-induced motions of a semi-submersible platform with four square columns, Part I: effects of current incidence angle and hull appendages. Ocean Eng. 54, 150–169.

Gonçalves, R.T., Rosetti, G.F., Franzini, G.R., Meneghini, J.R., Fujarra, A.L.C., 2013a. Two degrees-of-freedom vortex-induced vibration of circular cylinders with very low aspect ratio and small mass ratio. J. Fluid Struct. 39, 237–257.

Gonçalves, R.T., Rosetti, G.F., Fujarra, A.L.C., Oliveira, A.C., 2013b. Experimental study on vortex-induced motions of a semi-submersible platform with four square columns, Part II: effects of surface waves, external damping and draft condition. Ocean Eng. 62, 10–24.

Gonçalves, R.T., Franzini, G.F., Rosetti, G.F., Meneghini, J.R., Fujarra, A.L.C., 2015. Flow around circular cylinders with very low aspect ratio. J. Fluid Struct. 54, 122–141.

Gonçalves, R.T., Fujarra, A.L.C., Rosetti, G.F., Kogishi, A.M., Koop, A., 2018. Experimental study of the column shape and the roughness effects on the vortex-induced motions of deep-draft semi-submersible platforms. Ocean Eng. 149, 127–141.

Huang, N.E., Shen, Z., Long, S.R., Wu, M.C., Shin, H.H., Zheng, Q., Yen, N.C., Tung, C.C., Liu, H.H., 1998. The empirical mode decomposition and the Hilbert spectrum for nonlinear and non-stationary time series analysis. Proc. Roy. Soc. Lond. 454, 903–995.

Jauvtis, N., Williamson, C.H.K., 2004. The effect of two degrees of freedom on vortex-induced vibration at low mass and damping. J. Fluid Mech. 509, 23–62.

Leong, C.M., Wei, T., 2008. Two-degree-of-freedom vortex-induced vibration of a pivoted cylinder below critical mass ratio. Proc. Math. Phys. Eng. Sci. 464 (2099), 2907–2927.

Liu, M., Xiao, L., Lu, H., Shi, J., 2016. Experimental investigation into the influences of pontoon and column configuration on vortex-induced motions of deep-draft semi-submersibles. Ocean Eng. 123, 262–277.

Liu, M., Xiao, L., Liang, Y., Tao, L., 2017. Experimental and numerical studies of the pontoon effect on vortex-induced motions of deep-draft semi-submersibles. J. Fluid Struct. 72, 59–79.

Morse, T.L., Govardhan, R.N., Williamson, C.H.K., 2008. The effect of end conditions on vortex-induced vibration of cylinders. J. Fluid Struct. 24, 1227–1239.

Norberg, C., 1994. An experimental investigation of the flow around a circular cylinder: influence of the aspect ratio. J. Fluid Mech. 258, 287–316.

Okamoto, T., Yagita, M., 1973. The experimental investigation on the flow past a cylinder of finite length placed normal to the plane surface in a uniform stream. Bulletin of JSME 16 (95), 805–814.

Pesce, C.P., Fujarra, A.L.C., 2000. Vortex-induced vibrations and jump phenomenon: experiments with a clamped flexible cylinder in water. Int. J. Offshore Polar Eng. 10, 26–33.

Rahman, M.A.A., Thiagarajan, K.P., 2015. Experiments on vortex-induced vibration of a vertical cylindrical structure: effect of low aspect ratio. Int. J. Automot. Mech. Eng. 11, 2151–2530.

Rahman, M.A.A., Leggoe, J., Thiagarajan, K., Mohd, M.H., Paik, J.K., 2016. Numerical simulations of vortex-induced vibrations on a vertical structure with different aspect ratios. Ships Offshore Struct. 11, 405–423.

Sakamoto, H., Arie, M., 1983. Vortex shedding from a rectangular prism and a circular cylinder placed vertically in a turbulent boundary layer. J. Fluid Mech. 126, 147–165.

Sanchis, A., Saelevik, G., Grue, J., 2008. Two-degree-of-freedom vortex-induced vibrations of a spring-mounted rigid cylinder with low aspect ratio. J. Fluid Struct. 24, 907–919.

Sarpkaya, T., 2004. A critical review of the intrinsic nature of vortex-induced vibrations. J. Fluid Struct. 19, 389–447.

Someya, S., Kuwabara, J., LI, Y., Okamoto, K., 2010. Experimental investigation of a flow-induced oscillating cylinder with two degrees-of-freedom. Nucl. Eng. Des. 240, 4001–4007.

Stappenbelt, B., Lalji, F., 2008. Vortex-induced vibration super-upper response branch boundaries. Int. J. Offshore Polar Eng. 18, 99–105.

Sumer, D., 2013. Flow above the free end of a surface-mounted finite-height circular cylinder: a review. J. Fluid Struct. 43, 41–63.

Vikestad, K., Vandiver, J.K., Larsen, C.M., 2000. Added mass and oscillation frequency for a circular cylinder subjected to vortex-induced vibrations and external disturbance. J. Fluid Struct. 14, 1071–1088.

Wang, Y., Yang, J., Peng, T., Li, X., 2009. Model test study on vortex-induced motions of a floating cylinder. In: Proceedings of the 28th International Conference on Ocean, Offshore and Arctic Engineering, OMAE2009–79134. Honolulu, Hawaii, USA.

Williamson, C.H.K., Govardhan, R., 2004. Vortex-induced vibrations. Annu. Rev. Fluid Mech. 36, 413–455.

Williamson, C.H.K., Govardhan, R., 2008. A brief review of recent results in vortex-induced vibrations. J. Wind Eng. Ind. Aerod. 96, 713–735.

Zhao, M., Cheng, L., 2014. Vortex-induced vibration of a circular cylinder of finite length. Phys. Fluid. 26, 015111.